Design and manufacture of a proof-of-concept resorption heat pump using ammonia-salt chemisorption reactions

G.H. Atkinson [a,*], S.J. Metcalf [a], R.E. Critoph [a], G.S.F. Shire [a], M. van der Pal [b]

[a] Sustainable Thermal Energy Technologies Research Group, School of Engineering, University of Warwick, Coventry CV4 7AL, UK
[b] TNO Energy Transition, Westerduinweg 3, 1755 LE Petten, the Netherlands

ARTICLE INFO

ABSTRACT

Using the Large Temperature Jump (LTJ) experimental technique, alongside a review of the literature, sodium bromide (NaBr) and manganese chloride ($MnCl_2$) have been identified as a suitable working pair with ammonia refrigerant for a proof-of-concept resorption heat pump system. LTJ tests using a tube-side and shell-side unit cell reactor (sorption heat exchanger), show that the experimentally obtained equilibrium lines for adsorption and desorption of sodium bromide are: $\Delta H_{ADS} = 30{,}102.5$ J/mol; $\Delta S_{ADS} = 207.7$ J/(mol·K); $\Delta H_{DES} = 30{,}216.4$ J/mol; and $\Delta S_{DES} = 206.8$ J/(mol·K). Using a semi-empirical model, the NaBr composite salt (salt impregnated in expanded natural graphite (ENG)) has been characterised for use as a low temperature salt in a resorption heat pump, with manganese chloride as the high-temperature salt. The model constants, A and n, for adsorption are 1 and 3, and for desorption are 5 and 4 respectively for NaBr. Manganese chloride data has been previously reported (Hinmers et al., 2022). With an appreciation of the reaction dynamics and behaviour of the NaBr and $MnCl_2$ composite salts, a proof-of-concept resorption system has been designed and manufactured. The reactor design, alongside the overall experimental rig design (including data acquisition system) is reported. Initial filling and flushing tests show the success of the data acquisition and control system, and thus the overall suitability of the proof of-concept system for investigations into the coupled nature of ammonia salt reactions for a resorption heat pump application.

Introduction

The UK government is trialling the use of hydrogen for heating homes through a local neighbourhood hydrogen heating trial (to commence in 2023), and there are broader plans for low-carbon fuels (biogas and hydrogen) to replace fossil fuels in both industry and domestic settings (Government and Trevelyan, 2021; UK Government 2020). Important in achieving emissions targets will not only be the use of cleaner fuels, but also the development of more efficient heating and heat recovery systems which can reduce operational costs. Resorption systems using ammonia-metal halide salt (ammonia-salt) reactions have long been of interest and could offer carbon dioxide (CO_2) emissions reductions. As detailed by Alefeld (1975a; 1975b) metal halide salts are low-cost substances, and the reactions of ammonia-salts can be found over a wide temperature range, therefore allowing reactions to be tailored to different cycles and operating conditions. Hence, reversible ammonia-salt reactions present a comparatively inexpensive alternative to existing absorption systems, particularly in a resorption configuration

which removes the need for an evaporator and condenser. Pursuing research into developing ammonia-salt systems, such as a resorption heat pump where Gas Utilisation Efficiencies (GUEs, calculated from Eq. (2) in (Metcalf et al., 2021)) = 1.06 to 1.38 (for COPs in the range 1.2 to 1.6) can theoretically be achieved, compared to existing boiler technologies with GUEs = 0.85 to 0.9, could provide a low-cost, cleaner energy solution for domestic heating systems.

The methods and design of an ammonia-salt resorption heat pump are presented in this work. The same approach can be used for ammonia-salt refrigeration and heat transformation systems. For context, this paper builds on the work presented at the Heat Powered Cycles (HPC) conference (Hinmers et al., 2022), as well as a series of previous papers (Hinmers et al., 2022; Hinmers and Critoph, 2019; Atkinson et al., 2021; Hinmers et al., 2022) by the Sustainable Thermal Energy Technologies (STET) research group at the University of Warwick (Warwick). In recent years (Hinmers and Critoph, 2019; Atkinson et al., 2021; van der Pal and Critoph, 2017), the reversible chemical sorption reactions of ammonia refrigerant with halide salt adsorbents have been researched, because heats of reaction can be nearly double that of the latent heat of

---

Nomenclature

A	Arrhenius term (constant)	AB	reaction from type A to type B (salt A to B, or vice versa)
ΔH	reaction enthalpy change (J/kg)	ADS	adsorption
k	thermal conductivity (W/(m·K))	B	related to type B adsorbate with .B moles of ammonia
m	mass (kg)	BC	reaction from type B to type C (salt B to C, or vice versa)
n	pseudo-order of reaction (constant)	C	related to type C adsorbate with .C moles of ammonia
p	pressure (Pa, bar)	DES	desorption
R	universal gas constant (J/(kg·K))	ENG	expanded natural graphite
ΔS	reaction entropy change (J/(kg·K))	EQ	equilibrium
T	temperature (K)	H	high
t	time (s)	L	low
V	volume (m^3)	M	medium
X	advancement (from 0 to 1)	NH3	ammonia
		R	reaction (reaction heat)
Subscripts		S	sample
A	related to type A adsorbate with .A moles of ammonia	SALT	salt
		TM	thermal mass

vaporisation (Ziegler, 2009) and because of the potential for high ammonia uptakes into the halide salts — up to 1 kg ammonia per kg salt (Wang et al., 2014).

The work presented in this paper summarises the background and context of ammonia-salt reactions for resorption applications, the theoretical and experimental methods used in the identification of a suitable salt pairing for resorption and concludes with the preliminary results and discussion of a working proof-of-concept laboratory-scale resorption heat pump.

Resorption working principle

Resorption systems consist of two reactor vessels (reactors), each with a different salt (adsorbent) that reacts with ammonia refrigerant (adsorbate). The two reactors are connected to one another, allowing refrigerant flow between them, and are therefore at the same pressure. A resorption system works on the principle of different equilibrium temperatures at the same pressure, and a resorption heat pump operates between two pressures driven by three temperature levels.

The reactions of ammonia with salts in chemical sorption (chemisorption) are characterised as mono-variant in nature, where the reaction is driven by the pressure or temperature difference from the

equilibrium conditions (referred to commonly as the pressure or temperature equilibrium drop (Bao et al., 2018)), and can be represented by the Clapeyron equation, Eq. (1),

$$\ln\left(p_{EQ}\right) = -\frac{\Delta H}{R \cdot T_S} + \frac{\Delta S}{R}. \tag{1}$$

Fig. 1 illustrates the working principle of a single-effect resorption heat pump with a block diagram and Clapeyron diagram to explain the working cycle. For reference, the salt with the higher equilibrium temperature (at the same pressure) is termed the High-Temperature Salt (HTS), and the salt with the lower equilibrium temperature the Low-Temperature Salt (LTS). Goetz et al. (1993) provide useful descriptions for resorption heat pumps and other similar cycles.

Referring to Fig. 1:

1 During the high-pressure phase (p_H), high temperature heat (at T_H) is delivered to the HTS reactor, the salt desorbs (endothermic reaction) the adsorbed refrigerant causing the pressure to rise in the system. Simultaneously, as the pressure rises, the refrigerant, which can freely flow between the two linked reactors, starts to be adsorbed (exothermic reaction) in the LTS reactor, which starts initially in a fully desorbed state, i.e., there is no adsorbed ammonia. Once the
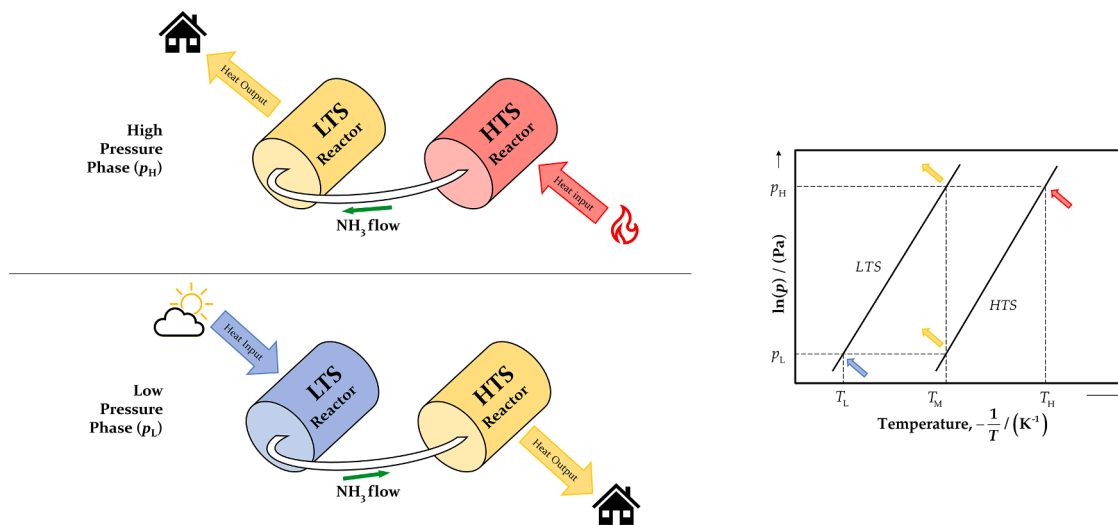

Fig. 1. (a) Block diagram of a resorption heat pump cycle during the high-pressure and low-pressure phases (p_H and p_L). (b) A Clapeyron diagram with the High-Temperature and Low-Temperature Salt (HTS and LTS) equilibrium lines plotted with the three defined temperature levels operating between two pressure levels depicted.

high-pressure phase conditions are reached, heat is delivered usefully (at T_M) to the home for domestic space heating or hot water purposes from the LTS adsorption reaction.

2 In the low-pressure phase (p_L), refrigerant flow is in the opposite direction to the pH phase. Desorption takes place in the LTS, which starts off fully adsorbed, using heat from ambient (at T_L) to drive the reaction and raise the pressure in the system. At the same time, adsorption takes place in the HTS, rejecting useful heat to the home (at T_M). As such, pseudo-continuous heating can be achieved by extracting the adsorption heat during both phases. However, for continuous heating two reactor pairs should be operated out of phase with one another.

As described previously in Atkinson et al. (2021), the temperature levels for a UK focused resorption heat pump system are well defined. The high temperature heat input, T_H, is the temperature of heat delivered by a gas burner (170-200 °C). The medium temperature heat output, T_M, needs to be sufficient to distribute hot water at 50 °C or above. Finally, the low temperature heat input, T_L, is provided by the environment, which for Coventry, UK can be considered in the range - 10 to + 10 °C.

As detailed by Yang et al. (2020), the pressure during the LTS desorption reaction in the low-pressure phase at the highlighted temperature range is critical to performance. Section 2.1 discusses salt choice for both the low-temperature and high-temperature salts, in addition to highlighting critical aspects to consider in selection.

Refrigerant

A discussion on salt selection is detailed in Section 2.1, but a note is made here as to refrigerant selection. Key desirable characteristics of a refrigerant are to have, amongst others, thermal stability, environmental harmlessness and it would ideally be non-toxic. Ammonia, methanol and water are frequently considered. Critoph (1989) considered ammonia and methanol to be the most suitable for refrigeration and heat pumping purposes, but with the instability of methanol above 120 °C, ammonia was determined to have the best potential for a heat pump system. Although toxic, ammonia systems compared to both water and methanol, tend to operate at, or above, atmospheric pressure which is a benefit for mass transfer (Yang et al., 2020).

Literature review

The literature review details the origins of ammonia sorption before summarising examples of experimental works using ammonia-salt reactions.

The chemical adsorption of ammonia with a halide salt was first noted by Faraday in 1823 when conducting an experiment with ammonia and silver chloride (Faraday, 1823). Although heat was produced during the reaction, with the abundance of fuel and reliable electrically driven vapour compression cycles (Critoph, 2012) through the 20th century, the development of solid sorption heat systems (storage, refrigeration, transformation and heat pumping) did not advance until the 1970/80 s in response to energy crises.

Goetz et al. (1997) was one of the first researchers to use the term "resorption" in the context of solid sorption. In their paper a $BaCl_2/NiCl_2$ resorption refrigerator (and air conditioner) was experimentally tested and simulated. The resorption system tested was subject to pressures of less than 1 bar, and the salts were hosted in a graphite matrix of 5–8 W/(m·K). The paper provides a useful summary of selection criteria (elaborated on in this work in Section 2.1), as well as detailing the coupling of the heat transfer and reaction kinetics for a sorption system. Of importance in the paper is the concluding remarks of pressure equilibrium drops at low pressures becoming the limiting process in the experimental work – a comment reiterated by subsequent researchers.

The mass of salt involved in Goetz's experiment was in the order of tens of grams in comparison to that of the experimental work by Lepinasse et al. (2001), who assembled a system containing 0.4 kg of $PbCl_2$ (LTS), coupled with 0.2 kg of $MnCl_2$ (HTS) for cooling applications – more comparable in mass to the work conducted in this paper. Lepinasse used a resorption cycle solely for cooling, but by using $PbCl_2$ as the LTS, although cooling production could be achieved at below 0 °C, a low cooling capacity was achieved because of the heavy molecular weight of $PbCl_2$.

Vasiliev et al. (2004) develop a resorption 'heat pump' based on $BaCl_2/NiCl_2$, in a four reactor configuration, for specific delivery of high temperature heat (steam at $T = 120 - 130$ °C) and chilled water ($T = 3-5$ °C). The salt in the experiment was embedded in a carbon fibre matrix to ensure fast heat and mass transfer to the reactive salt, as well as ensuring distribution of the salt throughout the matrix structure. Vasiliev summarises that the low thermal conductivity of the salt and high expansion factor of the reaction with the gas are two important aspects that can reduce heat pump performance. Worsøe-Schmidt (1983), in an earlier paper, detailed the procedure for embedding $CaCl_2$ in Portland cement, amongst other alternative solutions, to avoid significant swelling and contraction of the salt during the adsorption and desorption reactions. Gordeeva and Aristov (2012) summarise the importance of targeted design of composite salts inside porous matrices, addressing synthesis method, salt content and pore size. Additionally, the paper discusses the advantage of embedding $BaCl_2$ in expanded natural graphite to prevent agglomeration and improve heat transfer to the reactive salt.

Embedding or impregnating salt in a matrix was the technique used by van der Pal et al., where a metal foam was used as the matrix in a $LiCl_2$ (LTS) and $MgCl_2$ (HTS) resorption thermal transformer system (van der Pal et al., 2009). The system tested was cycled over 100 times and showed good cycle stability, however, with cycling times of nearly one hour being insufficient to complete the reaction and a lower than expected (estimated) thermal conductivity of the metal foam with salt matrix, van der Pal and Critoph (2017) investigated a salt impregnated in Expanded Natural Graphite (ENG). $CaCl_2$ was used as the salt in a single reactor setup with a condenser and evaporator, for which the main conclusion was that the salt in ENG exhibited little to no hysteresis for the 4–8 reaction in both adsorption and desorption. Hinmers and Critoph (2019) and Atkinson et al. (2021), also used ENG in their testing of a number of different salts for resorption heat pump and heat transformation applications, concluding the ENG is a highly porous and conductive structure that reduces agglomeration and shows promise for resorption systems with short cycle times.

Oliveira et al. (2009) used a $NaBr/MnCl_2$ salt pairing for an air conditioning system driven by low-grade heat. The salts were impregnated in a graphite matrix (powder) and then consolidated into blocks. The salt pairing presented matches the work in this paper but focused on air conditioning and simultaneous heat and cold production. One of the main conclusions drawn from the work was that the ratio of metal (thermal mass) to the composite powder was too high and had a detrimental effect on the COP and cooling power of the system – for any solid sorption reactor this is a vital metric to monitor to attain a suitable power output.

Li et al. (2010) continue work investigating $BaCl_2$ and $MnCl_2$ from Li et al. (2009), but this work focuses on the application in refrigeration, with comparisons drawn between adsorption and resorption cycles. 157 g of $MnCl_2$ and 130 g of $BaCl_2$ are employed in the same reactor configuration as detailed in prior work by the same authors and using the same consolidated compound technique from Oliveira et al. (2009). For the same temperatures tested, the resorption refrigeration cycle is reported to have achieved shorter cycles times, which is attributed to the beneficial equilibrium drop conditions to drive the reactions. Limited dynamic data is used to report the COPs and only broad comparisons are drawn over the variation in COP resulting from the change in conversion of the reactions.

In a later work, Li et al. (2011, 2013) investigate theoretically the principle of a two-stage desorption in the high-pressure phase of an

adsorption cycle, to lower the regeneration temperature. The work progresses and proposes a four-stage desorption cascading cycle, which seems at odds with the prior work on a simple adsorption cycle. If the prior work cannot prove the suitable utilisation of ammonia-salt reactions, then there is little point in pursuing a more complex cycle where thermal masses and sensible heats also scale with the increase in complexity. Li et al. (2013) also highlight that, for resorption systems, the heat output temperature fluctuates due to the oscillation of working pressure caused by the mismatch of the desorption and adsorption reaction rates. Thus, it is difficult to keep a good match between demand and supply. An interesting characteristic of note when designing a system.

Finally, Yang et al. (2020) provide a useful summary paper on sorption systems for "cold-climate heating". In the paper, issues such as agglomeration, hysteresis, LTS desorption vapour pressure and matrix material are summarised, as well as a table detailing the experimental resorption systems of interest. Vasiliev and Oliveira are referenced (above) alongside work presented by Xu et al. (2011), for a $NH_4Cl/MnCl_2$ pairing. Although the reported COPs by Xu are reasonable, the specific powers achieved are low, because one half cycle (high-pressure phase or low-pressure phase) was 6 h – i.e., 12 h for a complete cycle.

Summary

To summarise, ammonia-salt reactions in a resorption configuration offer a less complicated system compared to a traditional sorption system (evaporator and condenser are replaced with a second adsorbent reactor) (Vasiliev et al., 2004). However, crucial to the successful realisation of these systems is the suitable design of a reactor (solid-gas heat exchanger) that overcomes heat and mass transfer limitations; therefore providing a good COP and specific power output (Goetz et al., 1993; Groll, 1993).

The work presented here has taken an empirically informed approach to the design and manufacture of a proof-of-concept resorption heat pump. The LTS selected for the test aims to improve performance of the low vapour pressure desorption reaction, and both the LTS and HTS are impregnated into a highly conductive ENG matrix to ensure good heat transfer into the dispersed salt crystals.

Although interest in sorption systems has grown significantly in recent years, there are a comparatively limited number of systems that have been taken to proof-of-concept completion and formally tested, and those that have often see issues with the designed reactor thermal mass and system cycle times. The research presented therefore aims to prove a sorption reactor (heat exchanger) design for ammonia-salt reactions that can achieve quick adsorbent cycling with a good COP and specific power output.

Materials and methods

Salt selection

To determine a suitable salt working pair for the proposed ammonia-salt resorption system, the following factors need to be taken into consideration:

- Defined temperatures based on application
- Pressure levels
- Salt ammonia uptake, density and overall suitability for use (e.g., toxicity, hazards)

Using the temperature levels defined in Section 1.1, and the ammonia-salt equilibrium data for halide salts from (G.L. An et al., 2019; Neveu and Castaing, 1993; Lepinasse and Spinner, 1994; Li et al., 2014), a figure can be generated to inform salt pairing selection based on end-use application, Fig. 2. The basis of this temperature constraint methodology can be found in Neveu and Castaing (Neveu and Castaing, 1993), but the additional analysis in considering uptake, density and solubility is vital for understanding in the design of a resorption system using a composite salt adsorbent.

A note at this point on the advantage of resorption systems employing paired salts, rather than a salt paired with a condenser and evaporator. Not only does resorption remove the need for the expensive condenser/evaporator components, but resorption is theoretically simple with only two connected reactors; as can be seen in Fig. 2, there are also many salts which can be selected based on application. Finally,
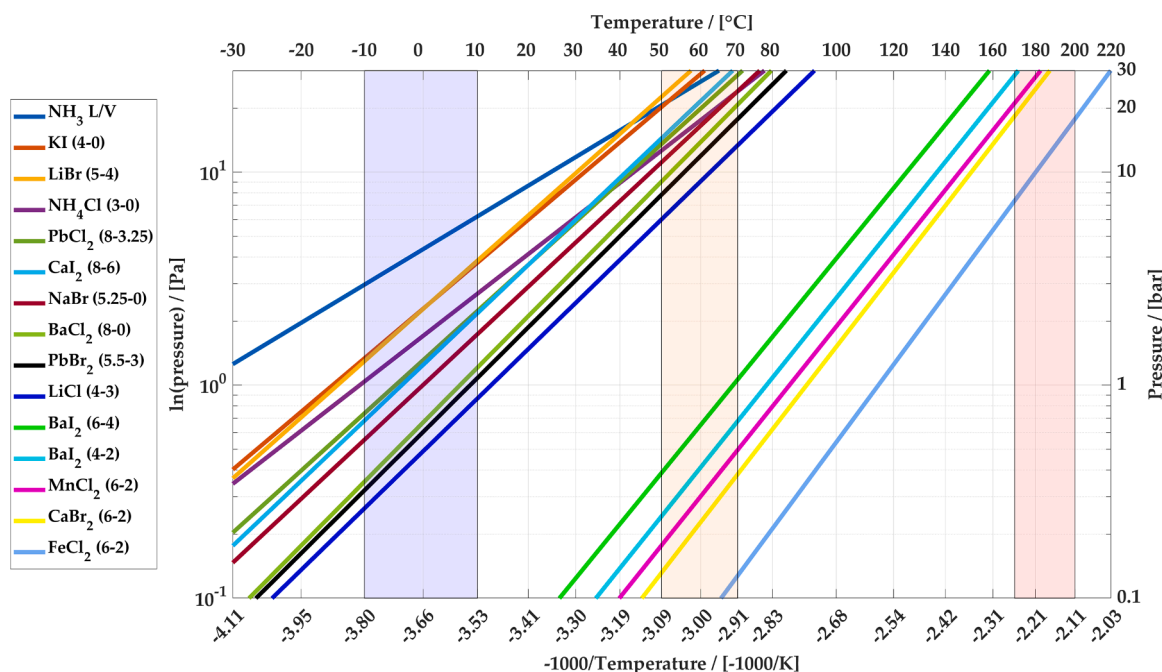

Fig. 2. Plot of ln(pressure) vs. −1000/Temperature, with the temperature bands, T_L (blue, left), T_M (orange, centre) and T_H (red, right) highlighted from Section 1.1. See Appendix A, Table 5. The legend works from left to right in the plot.

Table 1

Selected Low-Temperature Salt (LTS) information to inform selection in a resorption heat pump cycle with the three defined temperature levels.

Salt (Mole change)	M.W. (g/mol)	Reaction Heat (ΔH)/(J/mol)	NH_3 Uptake (kg_{NH3}/kg_{SALT})	Salt per kg_{NH3} (kg_{SALT})	Density (kg/m^3)	V_{SALT} per kg_{NH3} (L)	V_{RATIO} ($BaCl_2$ basis) (-)	Water Solubility at 20 °C (/100 mL)
KI (4–0)	166.00	32,015	0.410	2.437	3120	0.78	1.97	140.00
LiBr (5–4)	86.85	33,689	0.196	5.099	3464	1.47	3.71	166.70
NH_4Cl (3–0)	53.49	29,433	0.955	1.047	1519	0.69	1.74	37.20
$PbCl_2$ (8–3.25)	278.10	34,317	0.291	3.438	5850	0.59	1.48	0.99
CaI_2 (8–6)	293.89	35,991	0.116	8.628	3960	2.18	5.50	66.00
NaBr (5.25–0)	102.89	35,363	0.869	1.151	3210	0.36	0.90	90.80
$BaCl_2$ (8–0)	208.23	38,250	0.654	1.528	3856	0.40	1.00	35.80
$PbBr_2$ (5.5–3)	367.01	39,758	0.116	8.620	6660	1.29	3.27	0.97
LiCl (4–3)	42.39	36,828	0.402	2.489	2070	1.20	3.03	78.50

compared to pairing a HTS with a condenser/evaporator, a resorption system will operate at lower pressures. Take for example a medium temperature heat output at 60 °C, to condense ammonia the pressure is over 26 bar, whereas employing a salt such as sodium bromide (NaBr), the working pressure at the same temperature is around 12.5 bar, providing an inherent safety aspect.

As detailed in Yang et al. (2020) one of the major limiting factors when considering a salt pairing for resorption heat pump applications is the ability of the LTS to desorb at low vapour pressures.

Using Table 1 and Fig. 2, when considering the: reaction temperatures; the uptake of the ammonia refrigerant onto the salt; hazards; and the need to design a compact reactor, the salts ammonium chloride (NH_4Cl), lead chloride ($PbCl_2$), sodium bromide (NaBr) and barium chloride ($BaCl_2$) can be considered as suitable LTS candidates. Lead chloride is not considered further because of the hazards of using the salt, as well as poor solubility in water, which is important for the composite salt production method, Section 2.2.

Comparing NH_4Cl, NaBr and $BaCl_2$, Hinmers and Critoph (2019) review the ammoniation of barium chloride and conclude that the salt is suitable for resorption heat transformation applications. However, in a resorption heat pump application during the low-pressure phase using an ambient heat input (T_L), the desorption reaction of $BaCl_2$ as a LTS would be at sub-atmospheric pressure, which would impact mass transfer during the reaction. Working at below atmospheric pressure not only causes mass transfer issues, but there is also the necessity to maintain a leak-free negative pressure system as any inward leak of air into the closed ammonia system could impact performance. NaBr and NH_4Cl on the other hand offer desorption temperatures of 0 °C at, or above, atmospheric pressure. Atkinson et al. (2021) discuss the performance of ammonium chloride, but highlight issues associated with uptake into the composite matrix. When comparing tests conducted with NaBr using the same methods as described by Atkinson et al., because of the increased solubility in water, greater uptakes into the composite sample could be achieved, without seeing the impact of mass transfer on the results. In other words, the pressure changes are linear during the isothermal phase change indicating a heat transfer limited process, Section 3, whilst still maintain a high salt-to-ENG ratio.

Based on the analysis above, as well as the discussion outlined in Yang et al. (2020), $MnCl_2$ was selected as the high-temperature salt.

Composite material preparation

The $MnCl_2$ and NaBr halide salts are impregnated in an Expanded Natural Graphite (ENG) matrix to address both conductivity issues with the salt adsorbent, as well as to reduce swelling or agglomeration of the salt (van der Pal and Critoph, 2017; Hirata and Fujioka, 2003).

The ENG sheet, from which hexagonal or round disks are manufactured, is a 10 mm thick SIGRATHERM graphite lightweight board of 150 kg/m^3 density. For tube-side LTJ tests, round disks which fit the internal diameter of a ½'' tube are manufactured. The round disks, Fig. 3, have a 1 mm central hole drilled for gas transport through the reactor (Hinmers

and Critoph, 2019; Atkinson et al., 2021). For shell-side LTJ tests, hexagonal samples of 32 mm across flats (16 mm apothem) with a central hole to fit over a ½'' tube are manufactured (Hinmers et al., 2022).

After manufacture of the ENG disks (round or hexagonal), the method depicted in Fig. 3 is followed to produce the composite salt samples for either NaBr or $MnCl_2$.

The ENG disks are dried in an oven for a minimum of 30 min at 200 °C, Fig. 3(a), and then weighed immediately to avoid moisture uptake and to determine the 'pure' ENG mass, Fig. 3(b). The dried disks are then submerged in a salt solution, the strength of which predominantly determines the salt uptake. The disks in salt solution are placed under vacuum conditions in a chamber for 24 h, Fig. 3(c), removed and finally dried in an oven to evaporate the water resulting in the final composite salt samples (composite samples or samples), Fig. 3(d). The sample mass is measured and compared with the 'pure' ENG mass to assess the salt uptake into the ENG matrix. An example of the hexagonal composite samples produced using the same method are shown in Appendix B, Fig. 25.

After the second weighing to determine the salt uptake into the pure ENG, the samples (either tube-side round, or shell-side hexagonal) are placed in the appropriate reactor, Section 2.3.1, ready for Large Temperature Jump (LTJ) analysis.

Experimental and analysis method

Large temperature jump

The Large Temperature Jump (LTJ) technique has been used to assess composite salt characteristics in previous work at Warwick (Hinmers et al., 2022; Hinmers and Critoph, 2019; Atkinson et al., 2021; van der Pal and Critoph, 2017) and was originally developed by Aristov et al. (2008). LTJ experiments place composite salt samples inside a reactor (adsorbent solid-gas heat exchanger), of representative 'unit cell' size, connected to a large expansion vessel ammonia reservoir. As previously mentioned, the composite samples can be placed in either a shell or tube-side configuration, where the 'shell' or the 'tube' refers to the location of the composite samples in the reactor. Silicone oil or water can be used as the heat transfer fluid, providing representative temperature heat inputs and flow conditions depending on the test conditions. The heat transfer fluid is supplied to the reactor at a set temperature from a pair of Huber Ministat 240/240 w temperature-controlled circulator baths, and the temperature 'jump' is imposed on the composite sample by setting the baths to different temperatures and controlling the flow to the reactor. The flow to the reactor is controlled with a pneumatically operated valve manifold. In the tube-side reactor, the heat transfer fluid flows through the annulus of a double-pipe heat exchanger around a central tube that houses the round disk composite samples, Fig. 4; in the shell-side reactor, the heat transfer fluid flows through a central tube, around which the hexagonal disk samples are pushed onto the tube, Fig. 5.

For the LTJ tests, once the composite samples are positioned in the reactor following the completion of the salt impregnation process, the
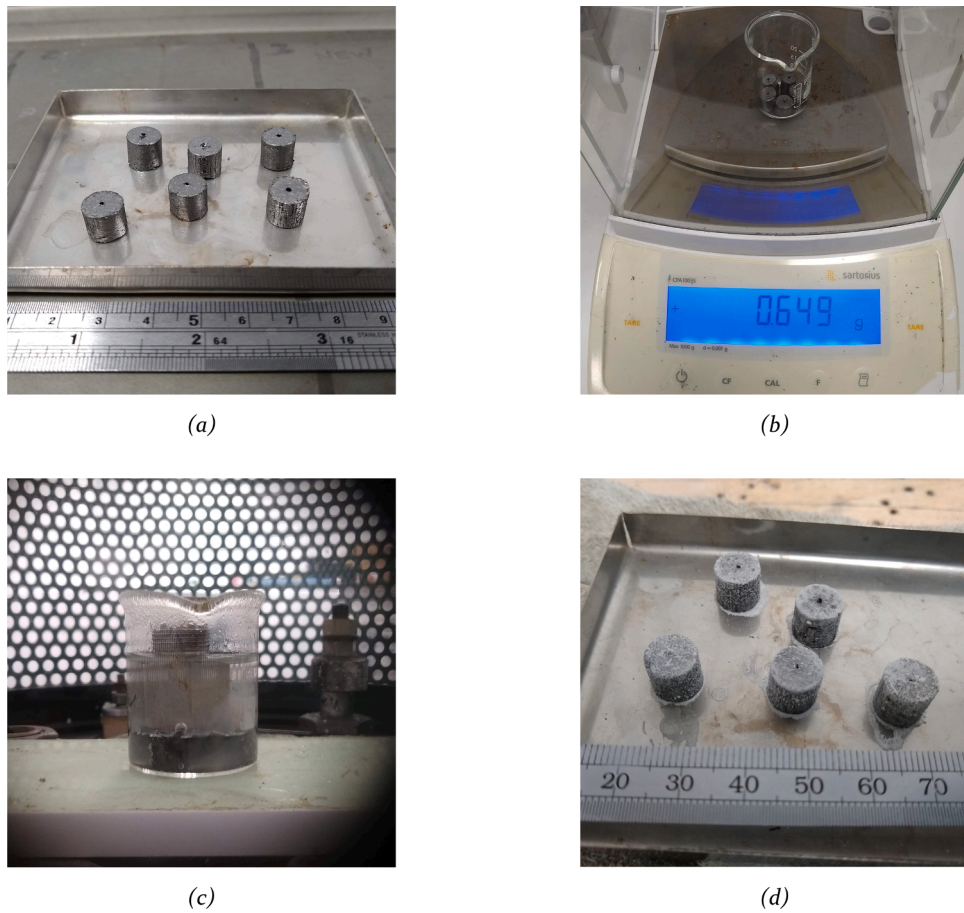
(a)

(b)

(c)

(d)

Fig. 3. (a) Dried ENG disk samples (central hole drilled for thermocouple access and gas transport) (b) the mass of the disks is measured (c) ENG disks submerged in salt solution under vacuum conditions and (d) the final composite samples.
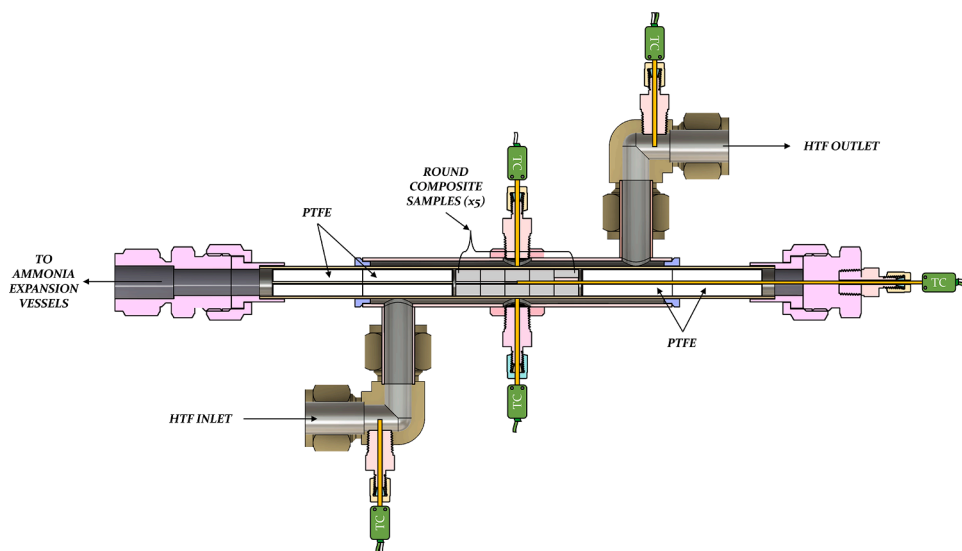

Fig. 4. A cross-section CAD image of the double pipe tube-side 'unit cell' reactor to house the round composite samples with a 1 mm central hole, Fig. 3(d). The composite salt is placed in the central tube as shown, with the heat transfer fluid (water or silicone oil) flowing through the annulus formed between the outer ¾'' shell and the central ½'' tube. The thermocouples (TC) are shown for completeness and the PTFE sections are used to reduce any 'dead' volume in the reactor to avoid pressure cycling (Atkinson et al., 2021).
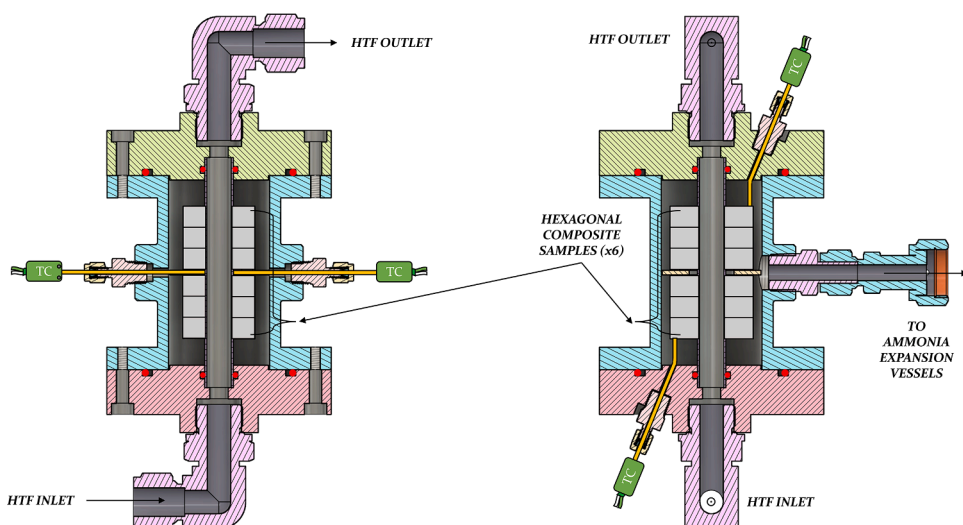
Fig. 5. A cross-section CAD image of the shell-side reactor with hexagonal composite samples placed around the central ½'' tube. (left) The front view of the reactor illustrating the position of the thermocouples (TC) which measure the tube wall temperature between the sets of composite samples, as well as showing the fluid inlet and outlet elbows. (right) A 90 ° rotated view to show the ENG TCs which are positioned in the flanges of the design, as well as the outlet on the shell-side to the ammonia expansion vessels.

ammonia-side is connected to the expansion vessels through a ½'' Swagelok VCO face seal fitting, and then the vessels and reactors are evacuated and heated to remove any air or moisture. The reactor is then isolated, and the expansion vessels filled with ammonia. The expansion vessel temperature (and by extension the insulated cabinet) is controlled with a separate temperature-controlled circulator bath that pumps water through hose wrapping surrounding the expansion vessels, Fig. 6. Once the expansion vessel pressure is stable and the reactor has reached the suitable temperature setpoint based on the salt being tested, the reactor and the composite samples are exposed to ammonia. From this point, a series of LTJ tests are conducted using published equilibrium data as a reference, and through the analysis method, Section 2.3.2, and mathematical model, Section 2.3.3, the sorption characteristics of the composite salt can be found.

The temperature and pressure sensors are connected to a National Instruments CompactDAQ for data acquisition, using LabView to display and save real-time data.

The LTJ experimental setup subjects the composite samples to realistic pressure and temperature changes inside a 'unit cell' reactor that are representative of a larger reactor design. The tests provide an indication of the performance of the composite salt by enabling the identification of model constants and an understanding of the dynamic performance by showing the onset temperature of the adsorption and desorption reactions at different pressures. The LTJ test can also be modified to estimate the 'true' heat of reaction by disconnecting the expansion vessels from the reactor. Unlike in a LTJ test, the temperature change must be slow, allowing the reaction to track along the equilibrium isostere. The slow nature of the test allows the reaction taking place to track up and down the equilibrium line and a single value for the enthalpy (or heat) of reaction can be found. A cycle (desorption and adsorption) using this method can take several hours compared to an LTJ test which can see the composite salt cycling in minutes (typically 5-20 min depending on the sample).

Analysis

For the LTJ recorded data, the temperature and pressure are used to find the adsorption and desorption equilibrium line which show the reaction onset as described by the Clapeyron equation, Eq. (1).
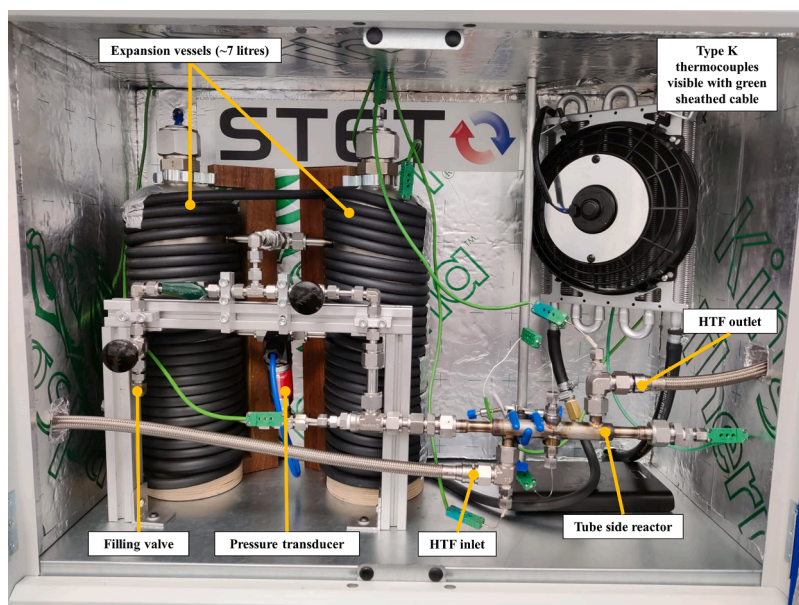

Fig. 6. Image of the Large Temperature Jump (LTJ) experimental setup in the tube-reactor configuration. An example of the shell-side setup can be seen in Appendix B, Fig. 26.
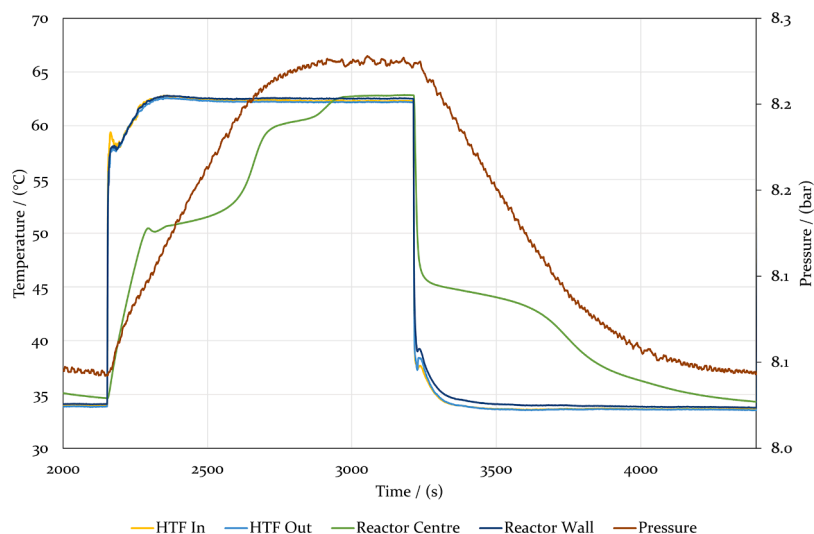
Fig. 7. An example of a tube-side reactor Large Temperature Jump (LTJ) output for sodium bromide. The tube-side wall, composite sample and Heat Transfer Fluid (HTF) temperatures are read from the left-hand y-axis and the system pressure from the right-hand y-axis. Plotted is a desorption reaction followed by an adsorption reaction, with the isothermal phase change regions clear on the green reactor centre temperature, during which there is a linear change in the pressure of the system.

An example of a complete LTJ cycle output is shown in Fig. 7 for a tube-side sodium bromide sample. The temperature of the tube-side wall (driving temperature), the centre composite sample temperature and the pressure for the system are plotted. A superheat region prior to the isothermal phase change can be seen in Fig. 7, mirroring the behaviour seen by Hinmers and Critoph (2019).

Fig. 8 shows an example of the same LTJ experiment for a shell-side test but note that the composite sample temperature is obtained from the two ENG thermocouples, touching the external surface of the samples, compared to a single thermocouple positioned in the centre of the samples for the tube-side reactor. The difference in setup can be seen in the cross-sectional images of the reactor in Section 2.3.1.

As detailed in Atkinson et al. (2021), to determine the reaction onset equilibrium lines, for each adsorption and desorption reaction at the pressure setpoints tested, multiple adsorption and desorption datasets

are analysed in MATLAB. Each dataset generates two linked graphs that provide the reaction onset conditions at a particular temperature and pressure, i.e., this generates one data point for an equilibrium line. By taking multiple points at each pressure across the tested range, the equilibrium points of the reaction can be plotted together on a single graph to be able to identify the equilibrium lines. An example of the linked data plots for an 8 bar adsorption reaction for a tube-side NaBr reaction is shown in Fig. 9. The results of the full analysis can be seen in Section 3.

From the derivation of the Clapeyron equation, the assumption is that the adsorption and desorption processes are reversible. However, if (irreversible) hysteresis is found for the sorption reactions, the reaction enthalpy change for the ammonia-salt reaction cannot be calculated from the gradient of the reaction (non-) equilibrium lines obtained from the analysis detailed here.
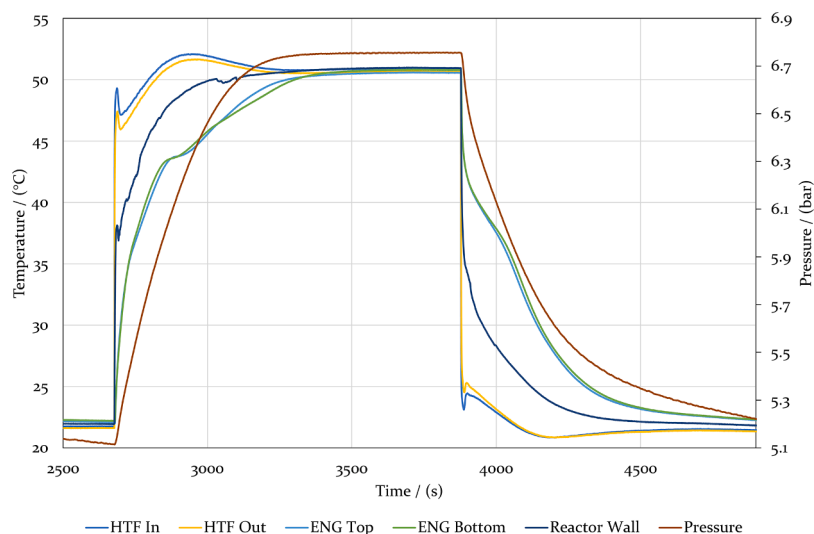

Fig. 8. An example of a shell-side Large Temperature Jump (LTJ) output for sodium bromide. The ENG top and bottom (composite sample), reactor wall and the Heat Transfer Fluid (HTF) temperatures are read from the left-hand y-axis and the pressure in the system on the right-hand y-axis. A desorption and adsorption reaction are plotted.
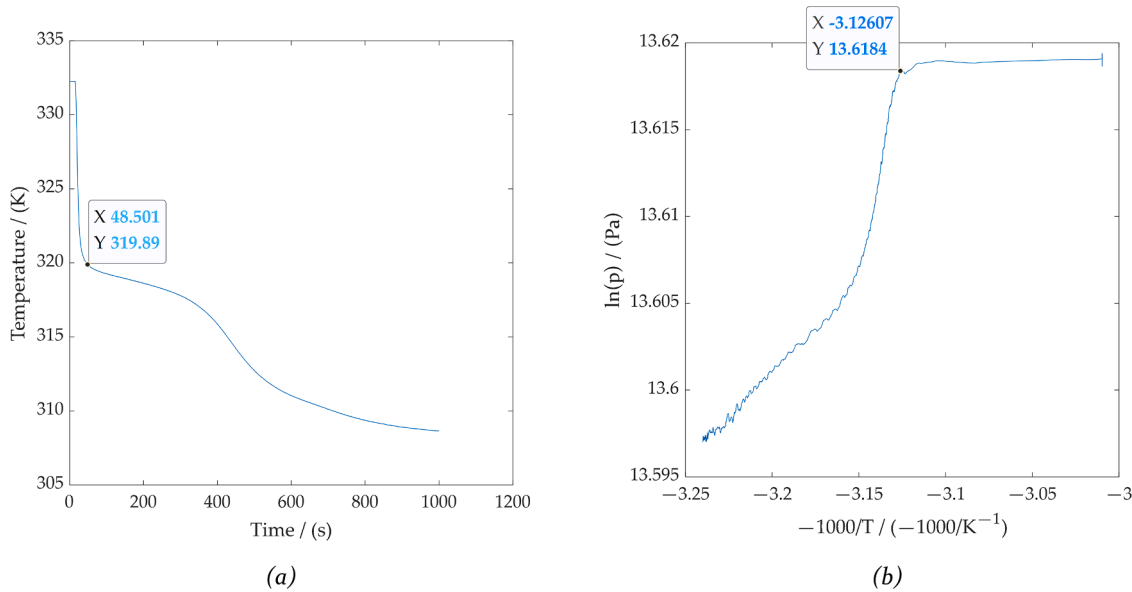
Fig. 9. An example of the two MATLAB plot outputs with a linked datatip readout for a NaBr tube-side adsorption reaction at approximately 8 bar with a temperature jump of 60 °C to 35 °C. (a) Plot of the composite sample temperature (K) against time (s) with the start of the isothermal phase change highlighted—in this case at 48.501 s and 319.89 K. (b) Plot of ln(p) (Pa) versus −1000/T (1000/K) with the onset of adsorption clear with a sharp change in ln(p) value indicating the onset of the adsorption reaction.

Mathematical model

The LTJ results, once acquired, are the input into an empirically informed heat transfer and reaction kinetics model developed by Hinmers et al. (2022), that enable the dynamic response of the composite salt samples to be understood. The reaction kinetics model is based on the linear form advancement equation summarised by Mazet, Amouroux and Spinner (Mazet et al., 1991), Eq. (2),

$$\frac{dX}{dt} = (1-X)^n A \frac{(p_{EQ}-p)}{p}. \tag{2}$$

Where: X is the advancement of the reaction (0 to 1); p is the pressure; p_{EQ} is the equilibrium pressure (calculated from the Clapeyron equation, Eq. (1)); and A and n are constants. Critoph et al. developed the advancement model into a physical adsorbent mass-based model, considering the mass of adsorbate in each state during the reaction. The main kinetic reaction equation for a single phase change (NaBr 5.25–0 and MnCl$_2$ 6–2) in the mass-based model is as follows for desorption,

$$\frac{dm_{SALTAtoB}}{dt} = (m_{SALTA}+m_{SALTB})\left(\frac{m_{SALTA}}{m_{SALTA}+m_{SALTB}}\right)^{n_{AB}} A_{AB}\left(\frac{p_{EQAB}-p}{p}\right) \tag{3}$$

and for adsorption,

$$\frac{dm_{SALTBtoA}}{dt} = (m_{SALTA}+m_{SALTB})\left(\frac{m_{SALTB}}{m_{SALTA}+m_{SALTB}}\right)^{n_{BA}} A_{BA}\left(\frac{p_{EQBA}-p}{p}\right) \tag{4}$$

where A and B refer to masses of adsorbent associated with $\cdot A$ mols and $\cdot B$ mols of adsorbed ammonia respectively. For sodium bromide, which reacts as $\cdot 5.25$ NH$_3$ - $\cdot 0$ NH$_3$, $A = 5.25$ and $B = 0$; for manganese chloride, which reacts as $\cdot 6$ NH$_3$ - $\cdot 2$ NH$_3$ for the reaction of interest in resorption heat pumps, $A = 6$ and $B = 2$.

Note that an assumption of the derivation of the Clapeyron equation is that the processes are reversible. This implies that if (irreversible) hysteresis is present the reaction enthalpy cannot be calculated accurately from the slope of the non-equilibrium reaction onset lines. Therefore, if results from the LTJ do not show a clear reversible process, then experiments need to be conducted with a minimal expansion volume to ascertain the 'true' heat of reaction (ΔH) for use in the Clapeyron equation and mathematical model, as described in Section 2.3.1.

Hinmers et al. (2022) detail the derivation of the adsorption and desorption heat transfer equations using an unsteady application of the first law for each composite sample control volume. The heat transfer model considers the change in internal energy of the composite sample (ENG and salt), ammonia adsorbate and gas within the volume, as well as the enthalpy flows of gas entering or leaving the reactor volume to the expansion vessel. Refer to the above reference for a summary of the equations which are not repeated for brevity.

In the mathematical model for each timestep, the temperature change in each control volume is calculated and a corresponding quantity of sensible heating and adsorption or desorption of ammonia is determined.

The model requires the identification of five modelling parameters to match the model output to the experimentally obtained LTJ data. The five parameters are:

1 Thermal conductivity of the ENG, $k_{ENG} = 26$ W/m·K, from the datasheet (SGL Carbon).
2 Wall heat transfer coefficient, characterised by an ammonia gas gap between the tube-side, or shell-side wall and the composite sample
3 Fraction of the salt accessible to the reaction, referred to as the active fraction
4 Arrhenius (A) constant term from Eqs. (2)-(4)
5 Pseudo-order of reaction constant term (n) from Eqs. (2)-(4).

Note that for 4 & 5, the constants are different for adsorption and desorption, but once identified the values remain constant across the pressure range tested.

Large temperature jump results

Low-Temperature salt – sodium bromide (NaBr)

Equilibrium line

Using the analysis methodology outlined in Section 2.3.2, by taking multiple adsorption and desorption reactions at different pressures, the reaction equilibrium onset can be identified by plotting the data points and drawing a line of best fit through the data. The result of this analysis can be seen in Fig. 10, where the adsorption and desorption reaction
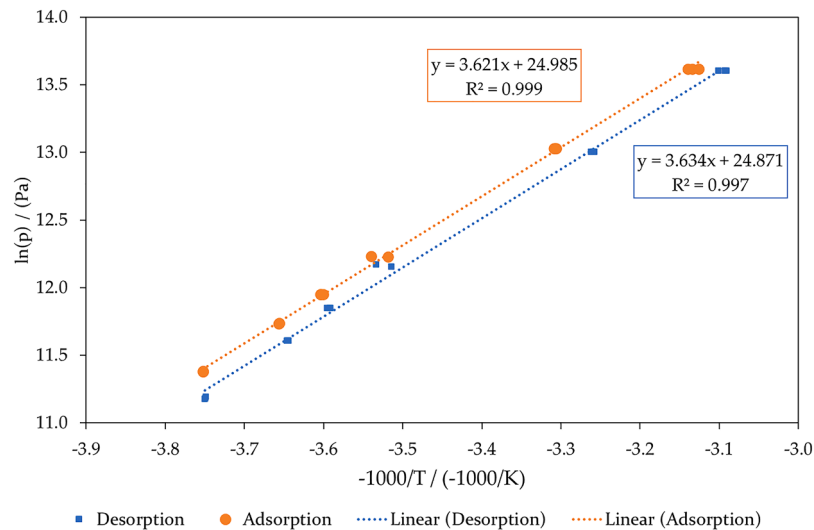
Fig. 10. Scatter graph for the adsorption (orange and round markers) and desorption (blue and square markers) across the sodium bromide tube-side sample set tested. A linear regression line (dotted line) is plotted through the data set; the fits of 0.999 and 0.997 respectively for adsorption (left) and desorption (right) indicate a strong positive correlation. The resulting line of best fit equation is also displayed, from which the ΔH and ΔS values are found.

onset can be clearly seen, with a small hysteresis band between the two. The region between adsorption and desorption has been well documented in previous research (Mazet et al., 1991; Furrer, 1980; Goetz and Marty, 1992; An et al., 2019), being referred to as a pseudo-equilibrium or hysteresis region. For sodium bromide this hysteresis has not previously been reported and is useful in understanding the reaction temperatures of the LTS in a resorption heat pump design.

For the heat of reaction, because of the parallel nature of the lines, when taking an average of the reaction enthalpies and entropies, a close match to the data obtained in Bao and Wang (2010) is found, providing confidence in the heat of reaction result. A graph showing the single heat of reaction 'true' equilibrium line is in Appendix C, Fig. 27.

The final values for the enthalpy and entropy of reaction onset and the overall heat of reaction for sodium bromide are:

Adsorption onset : $\Delta H_{ADS} = 30102.5$ J/mol; $\Delta S_{ADS} = 207.7$ mol·K.
Desorption onset : $\Delta H_{DES} = 30,216.4$ J/mol; $\Delta S_{DES} = 206.8$ mol·K. .
$\Delta H_{REACTION} = 30,159.5$ J/mol

Model outputs and equation constants

Table 2 shows the identified model parameters, Section 2.3.3, which match across the tube- and shell-side LTJ tests, with the graphical outputs from the program shown in the following tube-side and shell-side sections.

Table 2
Model constants used in the analysis of the sodium bromide LTJ tests. A and n remain the same for the tests, with the 'gap' changing because of the difference in the tests being conducted.

LTJ Test	Gas gap (influences the heat transfer coefficient)		A_{ADS}	n_{ADS}	A_{DES}	n_{DES}	Active Fraction
Tube-side	Adsorption: Desorption:	0.150 mm 0.125 mm	1	3	5	4	0.95
Shell-side	Adsorption: Desorption:	0.005 mm					

Tube-side. For the tube-side tests, the prepared round composite samples, Fig. 3(d), contained 0.656 g of ENG and 1.140 g of sodium bromide, with tests ranging from 0.8 to 8 bar.

With the identified model constants, Table 2, a selection of the MATLAB® model outputs for an 8 bar and 4.5 bar test in both adsorption and desorption are shown in Fig. 11.

In both adsorption and desorption, there is a good match regarding the reaction temperature, with the simulated isothermal phase change temperature matching closely to that of the experimentally obtained data. The difference in the gas 'gap' between adsorption and desorption, which characterises the heat transfer coefficient, is attributed to the swelling and contraction of the salt composite during adsorption and desorption inside the central tube.

Across the adsorption tests, the temperature and pressure profiles match well, whereas in desorption there are slight variations. In desorption, the match across the pressure change is good and the simulated pressure profile is representative of the experimentally observed data. At the beginning of the temperature profile, there is a difference in the simulated and experimental rise towards the isothermal phase change and, on arriving at the isothermal phase change, there is a superheat region in a similar way to that reported by Hinmers and Critoph (2019). Although present, the superheat region does not affect the ability of the model to predict the reaction temperature onset.

Following the phase change region in desorption, the simulated trend matches well to that of the experimental data. The experimental temperature profile does appear to indicate a second isothermal phase change region, however, there is not a corresponding change in the pressure rise as reported by Hinmers et al. (2022) for CaCl₂. Therefore, the reaction can be considered to be advancing as anticipated from 5.25 to 0 mol as reported in literature.

Shell-side. For the shell-side tests, the prepared hexagonal composite samples contained 4.643 g ENG and 7.952 g of sodium bromide. The tests were conducted with a CALGAVIN hiTRAN® tube insert to improve fluid to wall heat transfer and the pressure range tested was 3 to 8 bar.

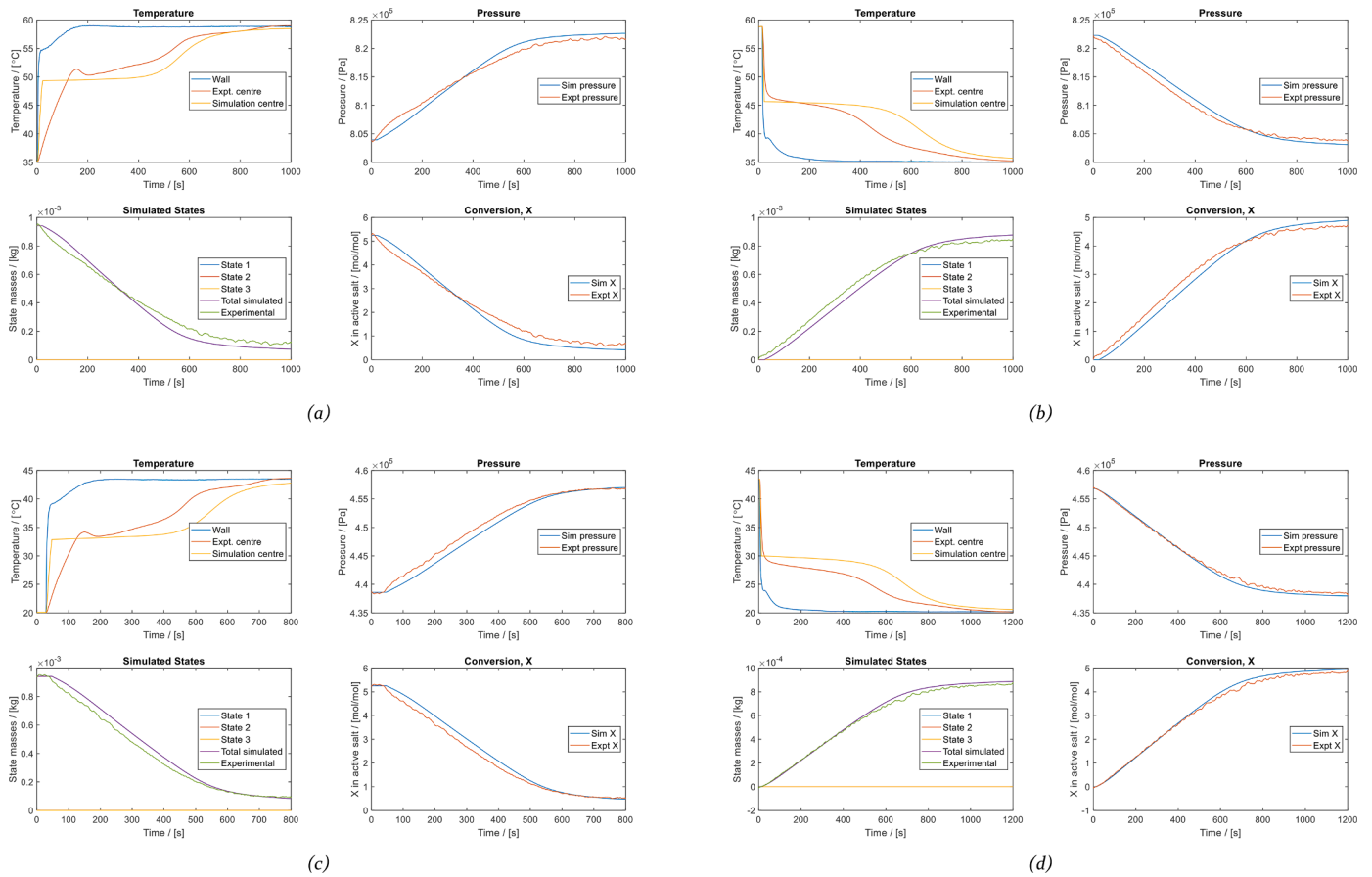The model constants remain the same from the tube-side to the shell-

Fig. 11. Model outputs for a tube-side LTJ test at: 8.0 bar in (a) desorption and (b) adsorption; and 4.5 bar in (c) desorption and (d) adsorption.
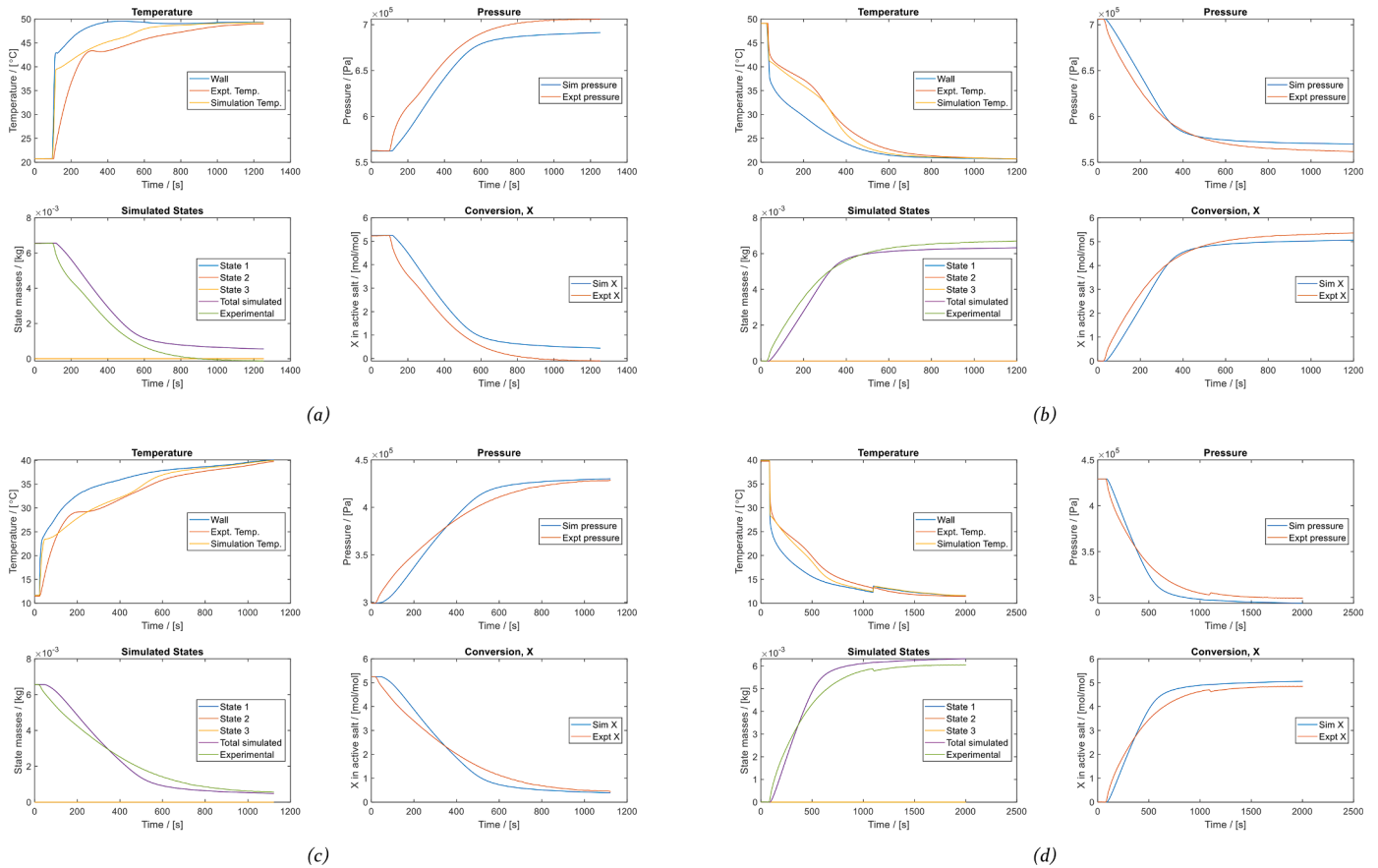

Fig. 12. Model outputs for a shell-side LTJ test at: 7.0 bar in (a) desorption and (b) adsorption; and 4.3 bar in (c) desorption and (d) adsorption.

Table 3

Model constants used in the analysis of the manganese chloride LTJ tests. A and n remain the same for the tests, with the 'gap' changing because of suspected swelling of the manganese chloride salt in the matrix.

LTJ Test	Gas gap (influences the heat transfer coefficient)		A_{ADS}	n_{ADS}	A_{DES}	n_{DES}	Active Fraction
Shell-side	Adsorption: Desorption:	0.032 mm 0.020 mm	2	3	3	3	0.8

side, providing confidence in the results. Pressure tests in the 5 to 7 bar and 3 to 4 bar range are shown for both adsorption and desorption in Fig. 12.

As with the tube-side tests, the reaction isothermal phase change temperature is predicted well with a match on the pressure rise, or fall, in desorption and adsorption respectively.

High-Temperature salt – manganese chloride (MnCl₂)

The equilibrium analysis for manganese chloride in the shell-side reaction has previously been published. Refer to the graphs plotted in (Hinmers et al. (2022), alongside the data published in Table 2 and Table 3 of the same work, some of which is repeated in Table 3 in this work for ease of reference. The enthalpy of reaction, model constants and details of the dynamic response of manganese chloride composite samples are reported.

Composite salt stability

From the tests across barium chloride (Hinmers and Critoph, 2019), ammonium chloride (Atkinson et al., 2021), calcium chloride (Hinmers et al., 2022), manganese chloride (Hinmers et al., 2022) and sodium bromide (this work), although swelling of the samples has been observed, across hundreds of LTJ cycles in adsorption and desorption there has been no evidence of agglomeration or composite salt performance degradation.

Additionally, from tests conducted by van der Pal and Critoph (van der Pal and Critoph, 2017) for a CaCl₂–NH₃ adsorption heat

transformer, for which the salt composite was manufactured with the same salt impregnation technique and ENG host matrix, there was no evidence of performance degradation from the salt composite. This provides confidence in adsorbent stability for future resorption tests, although future work, Section 6.1, should be conscious of any potential long-term performance changes during resorption testing.

Heat transfer enhancements

First, the 'fit' and contact of the hexagonal composite samples has been improved by creating a tighter fit of the samples over the ½'' tube. A tighter fit was achieved by manufacturing samples with a smaller central hole such that when pushing the samples onto the tube, the internal diameter of the sample was partially compressed. The progress towards a final central hole diameter was conducted methodically and is described in (Hinmers et al., 2022). In addition to improving the fit, to aid both the manufacturing process and the heat transfer from the tube to the composite samples, a graphite coating was applied to the outside of the tube wall. The application of the graphite spray provides a manufacturing improvement for the resorption reactor design, by providing a lubricating layer that reduces the failure rate of samples when being pushed onto the tube, Fig. 13(a). The graphite spray also provides a highly conductive coating onto the tube wall itself, as illustrated by Fig. 13(b), enhancing the heat transfer.

Second, the heat transfer from the fluid to the tube was also enhanced through introducing CALGAVIN hiTRAN® Thermal System tube inserts (CALGAVIN 2022) to the inside of the tube. For the single-phase fluid flow, the wire turbulators introduce turbulence into the flow regime to encourage greater mixing and therefore higher rate of heat transfer.

Theoretical performance

To assess the expected performance of the proposed resorption heat pump system, a number of calculations can be considered, first for the overall coefficient of performance (COP) for heating without considering the thermal mass of the system, and then also considering the composition of a unit cell, Fig. 14, of the proposed heat exchanger
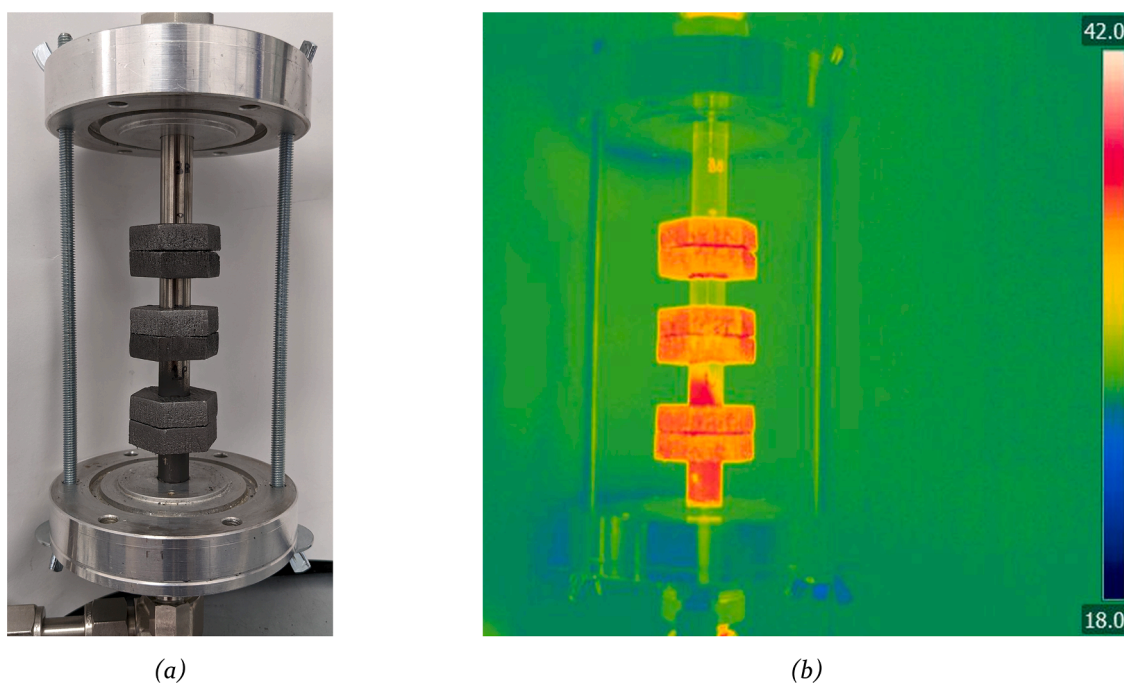
Fig. 13. (a) An image and (b) a thermal camera capture of the shell-side reactor setup without the central body section, Fig. 5 and Fig. 26. The flanges are secured with two lengths of threaded bar with water flow through the central tube in the same manner as normal LTJ shell-side tests.
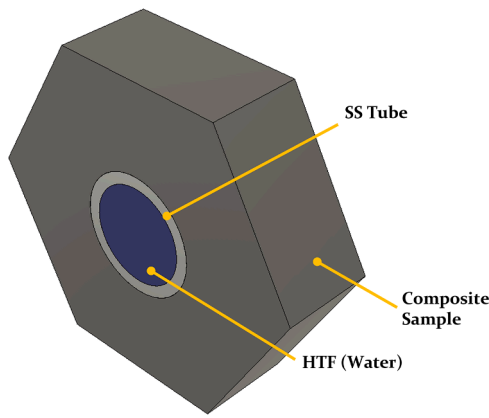
Fig. 14. ENG-salt and stainless steel 'unit cell' used in the COP calculations. The 16 mm apothem (32 mm across flats) composite sample fits over a ½'' (12.7 mm) stainless steel tube of 1.2 mm thickness, through which flows the heat transfer fluid (HTF), which in the case of the proof-of-concept resorption design is pressurised water.

design, Section 4.

The equation for the basic COP calculation for a single effect resorption system is (Vasiliev et al., 2004),

$$COP = \frac{Heat\ Ouput}{Heat\ Input} = \frac{\Delta H_{HTS} + \Delta H_{LTS}}{\Delta H_{HTS}} = 1 + \frac{\Delta H_{LTS}}{\Delta H_{HTS}}. \tag{5}$$

A unit cell of the reactor design is shown in Fig. 14, and a modified COP which considers the thermal mass of the stainless steel, water as well as gas heating, or cooling, provides a more complete analysis of the predicted performance at the defined temperature levels, Eq. (6). $Q_{\#R}$ refers to the reaction heat, $Q_{\#\#s}$ refers to the sensible heat required to raise the reactor thermal masses to the required temperature for reaction and $Q_{gas,\ hot\ or\ cold}$ is the heat required to raise or lower the temperature of the ammonia gas from one reactor temperature to the other. The numbers (#) are referring to the four numerically labelled points in Fig. 15 and an example of the calculated pressure and temperature conditions is shown in Fig. 16.

$$COP_{TM} = \frac{Heat\ Output_{TM+R}}{Heat\ Input_{TM+R}} = \frac{Q_{2R} + Q_{4R} + Q_{gas,\ hot} + Q_{34s}}{Q_{3R} + Q_{12s} + Q_{43s} + Q_{gas,\ cold}} \tag{6}$$

The ratio of salt to ENG, SS and water is based on the average

manufactured hexagonal sample placed in the reactor for the manufactured proof-of-concept resorption heat pump.

Raldow and Wentworth (1979) concludes that chemical heat pump systems are an easily regulated system (simple valve control in the gas line) and that since system energy is stored in chemical form the only thermal losses are that of sensible heat, which for small temperature differences are moderate. With this in mind, taking into account the thermal masses here in Fig. 16 and in the theoretical ideal 'second-law' COP calculation from Eq. (5), the 'second-law' efficiency obtainable from the system without heat recovery is 82% (=1.35/1.64), for these conditions.

Although 82% 'second-law' efficiency is promising as a technology, there will be further additional losses in the system. For example, the influence of the shell is not considered in the thermal mass analysis, so an anticipated drop in the performance of the resorption system is expected. To minimise the impact of the shell cycling, an internal folded sheet, Fig. 17, was incorporated into the sorption heat exchanger design, with the aim to reduce the heat loss from any gas flowing inside the triangular channels created by the hexagonally packed design inside the shell, Fig. 18. To monitor the shell cycling and therefore the influence on performance, surface thermocouples are adhered to the external surface of the shell with the change in temperature at lengths along the shell monitored to ascertain the extent to which the thermal mass of the shell changes in temperature.

Further details of the design and manufacture of a proof-of-concept resorption heat pump system, as well as the sorption heat exchanger design are discussed in the following section.

Design and manufacture

The reactor and overall rig design detailed in this section builds on the work summarised in Hinmers et al. (2022). In the paper by Hinmers et al., the identification of a 16 mm apothem (32 mm across flats) hexagon size around a ½'' (12.7 mm) tube was identified to attain the best COP values for a suitable specific mean power. A target of 1 kW/L was designed for, and the reactor cross-section is as depicted in Fig. 18.

Heat transfer enhancements for the sorption heat exchanger have already been discussed in Section 3.4, but the remaining details of the design are now discussed.

Reactors

The reactor design frontal cross section, which has the heat transfer
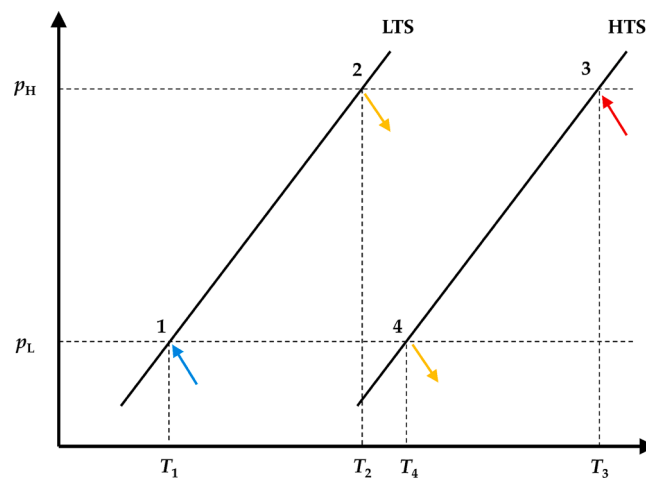

Fig. 15. Simple Clapeyron graph showing the ammonia-salt equilibrium lines for the low and high temperature salts with the four highlighted reaction points during the two pressure phases. The blue and red arrows at points 1 and points 3 show the low and high temperature heat inputs, and the amber arrows at points 2 and 4 show the medium temperature heat outputs.
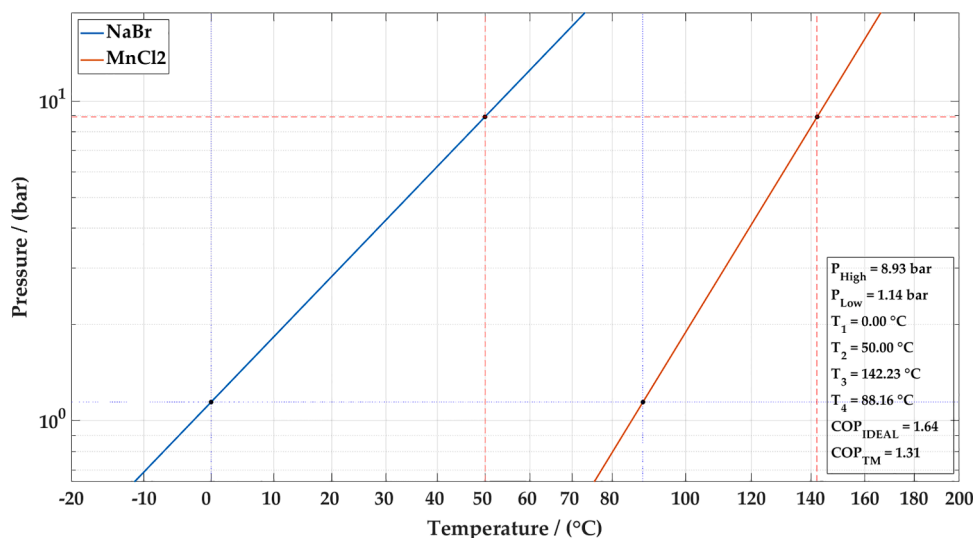
Fig. 16. Example output from resorption COP calculator using single heat of reaction lines for both salts on a Clapeyron diagram. COP$_{IDEAL}$ from Eq. (5) = 1.64, and considering thermal massed from Eq. (6), COP$_{TM}$ = 1.35.

fluid flowing through the tube-side and the composite samples on the shell-side (ammonia-side), can be seen in Fig. 18 and the longitudinal cross section in Fig. 19.

The overall design consists of seven identical hexagonal composite sample stainless steel tube sections packed into a stainless-steel shell. The tubes are ½'' in diameter with a 1.24 mm wall thickness. The composite samples are hexagonally cut to ensure a compact arrangement in the shell, with a 2 mm gas gap between each neighbouring hexagonal section – the design is as such to avoid mass transfer issues seen in similar reactor designs (Metcalf et al., 2021). Seven tubes are arranged inside a 4.5'' stainless steel shell. An endplate is welded to the tubes protruding at each end of the reactor to which a heat transfer fluid manifold plate is welded. The manifold has three aspects, the flat plate welded to the end of the seven tubes, an orifice plate to control the flow to the central tube and a channel plate that seals onto the flat plate with O-rings and distributes the pressurised water to all seven tubes. An endplate is welded to the inside diameter of the shell to create a com-

Fig. 17. Front view to the inside of the MnCl$_2$ HTS reactor prior to assembly. The folded sheet is visible and held in place by two rings at either end of the folded sheet section. The folded sheet aims to minimise heat loss by creating a stagnant ammonia gas layer at the inside face of the shell.
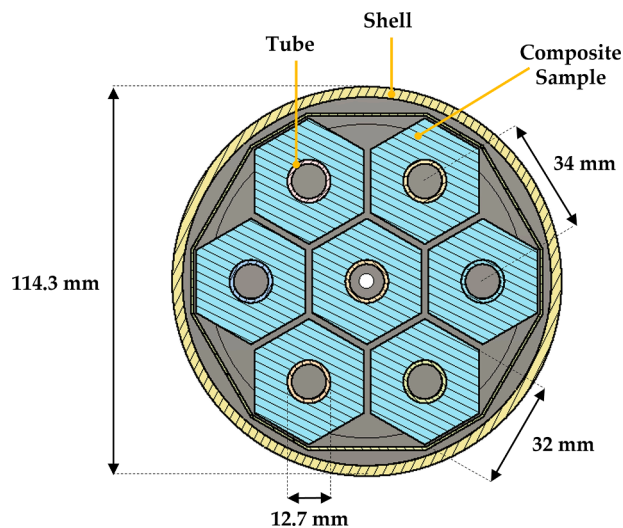

Fig. 18. Frontal cross section through the reactor showing the arrangement of the seven tubes, ENG and shell with key dimensions detailed.
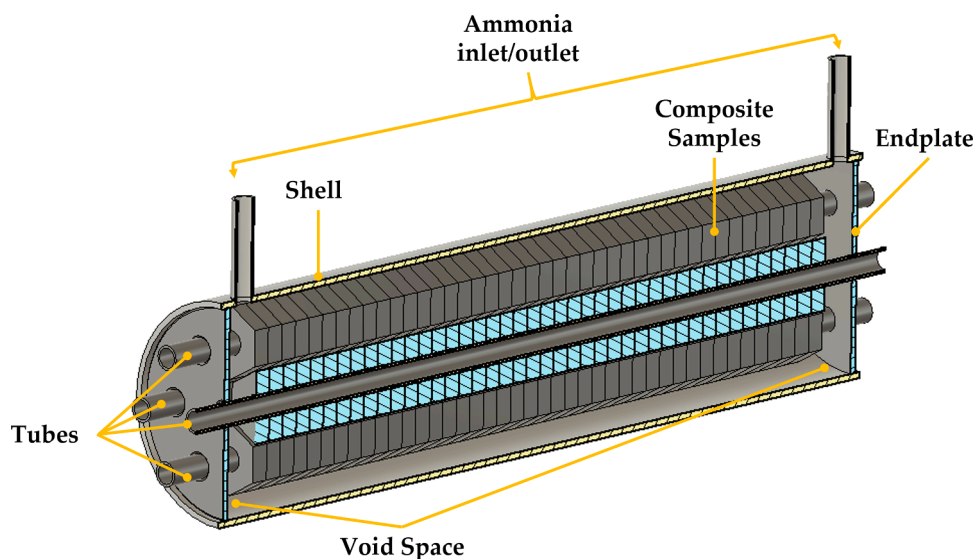
Fig. 19. An overall cross section through the reactor design showing the 3D view and the number of packed composite samples, the two ammonia outlets and the tubes in the endplates at the end of the shell.

plete pressure vessel, Fig. 19 and Fig. 20. The pressure vessel thickness (shell and endplates) has been designed for the pressures expected during resorption.

From the LTJ tests conducted, the reactions are completing in minutes (rather than hours seen in other research) and therefore when considering potentially high flow velocities of ammonia at low pressures and temperatures, when the density of the gas is at its lowest, an additional void space was added to improve the gas flow through the system. The void space also allows for any potential expansion of the composite samples during adsorption and desorption, as previously reported (Hinmers et al., 2022; Hirata and Fujioka, 2003). The 2 mm spacing between hexagonal sections also aids with any potentially high flow velocities of the ammonia during the reaction.

Manufacture

Manufacture of the reactors has involved two machining stages for the stainless-steel elements of the reactor to match the designed dimensions, as well as three welding stages.

The composite samples have been manufactured using the same method described in Section 2.2, with production scaled up to produce 180 samples at a time. The key reactor masses of interest are summarised in Table 4.

An example of a completed set of seven tubes with the composite samples in position around the central tube is shown in Fig. 20(a), with the arrangement inside the shell in Fig. 20(b). Each composite sample was pushed onto the tube individually, aided by the graphite spray layer on each tube for ease of manufacture.

Resorption rig

To incorporate the reactors in a resorption proof-of-concept system, a compact test rig has been designed to house the reactors and to analyse the performance. Fig. 21 shows the arrangement for the ammonia-side of the designed system, showing the arrangement of two salt reactors, an ammonia flow metre, pressure transducers and valves to shut off and fill the system.

On the fluid side, the system makes use of the ThermExS thermal test facilities at Warwick (Sustainable Thermal Energy Technologies (STET) 2019) to provide the desired temperatures and drive the resorption reactions. The fluid loops flow through a set of flow meters and the inlet and outlet temperatures to each of the reactors is also measured. The recording of the mass flow and temperatures on the inlet and outlet ensures an accurate heat balance can be calculated on the reactors.

The pressure transducers installed on the system have been deadweight pressure tested and the outputs from the Class A PT100s, used on the inlet and outlet of the fluid flow to the reactors, have also been checked at temperatures anticipated to be seen in resorption testing.

A LabView sensing and control program has also been developed to provide live monitoring and data logging of the temperatures, pressures and flow rates.

Overall, the system design provides a compact proof-of-concept test bench to be able to test modular reactor designs for both resorption heat pump and heat transformer applications. (Fig. 22).
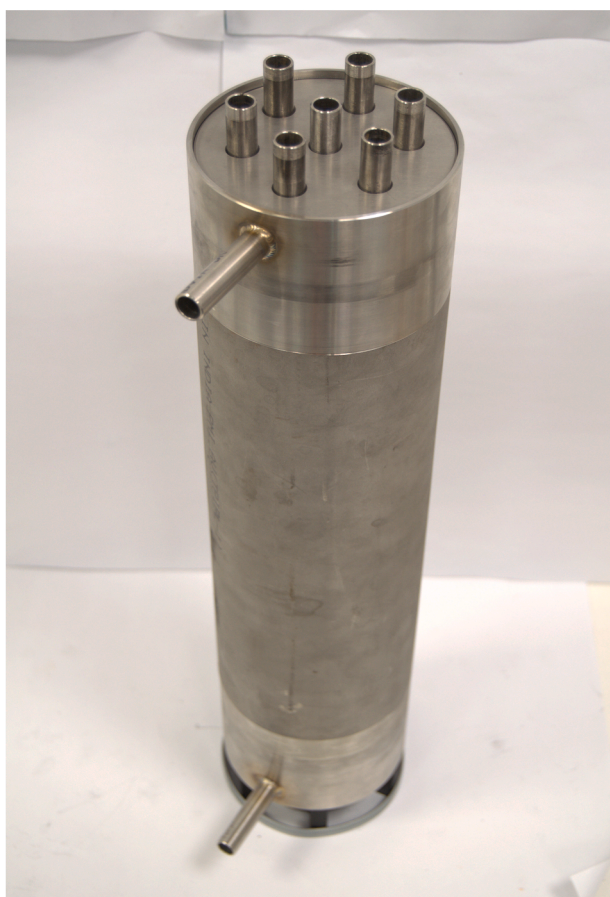
Data acquisition and initial ammonia fill

Sodium bromide reactor (LTS)

The first test of the proof-of-concept resorption test rig was in the

(a)

(b)

Fig. 20. (a) Image showing seven ENG-salt (composite sample) tubes for the NaBr low temperature salt reactor. For reference a single hexagonal composite sample is 32 mm across flats and approximately 9.5–10 mm thick and (b) the complete assembly arrangement prior to the first welding stage – for dimensions of the reactor refer to Fig. 18.

Table 4
Summary table detailing the key characteristics of the sodium bromide (LTS) and manganese chloride (HTS) reactors as manufactured.

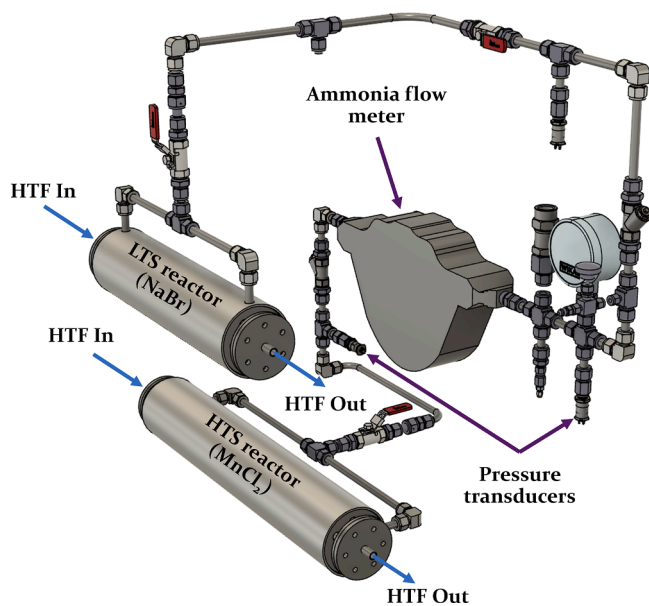| Reactor Detail	NaBr Reactor (LTS)		MnCl$_2$ Reactor (HTS)
Overall length / (m)	0.51		0.68
Shell mass / (kg)	3.28		4.88
Tube mass (7 tubes) / (kg)	1.23		1.65
Manifold mass (qty. 2) / (kg)		1.32	
Endplate mass (qty. 2) / (kg)		0.39	
Misc. masses / (kg)	0.47		0.61
ENG mass / (kg)	0.41		0.54
Salt mass / (kg)	0.63		0.86

Fig. 21. CAD layout of the ammonia-side connecting the two reactors to one another. The MnCl$_2$ reactor is situated beneath the NaBr reactor and the connecting pipework between them has a Coriolis flow metre, pressure transducers and a thermocouple to measure ammonia flow, pressure and gas temperature. The frame and heat transfer fluid (HTF) side have been omitted for clarity.

filling of the first manufactured reactor – the NaBr LTS reactor. The filling test gave an opportunity to control the temperature of the flow through the HTF-side of the reactor, whilst data logging the temperature and mass flow of the pressurised water through the system. Additionally, and more importantly, the ammonia mass flow readings were recorded to check that the fill mass measured on the scales from the ammonia bottle matched the integrated mass flow signal from the flow metre (within acceptable experimental expectations).

Fig. 23 shows the ammonia mass flow metre output during the flush, vacuum and filling procedures for the NaBr reactor.

Based on the mass change of the ammonia bottle on the weighing scales before and after filling, the mass of ammonia filled in the LTS reactor was 440 g$_{NH3}$. Based on the integration of the signal in Fig. 23, the filled mass was 439.2 g$_{NH3}$, less than a 1% difference. This result is very satisfactory, demonstrating the accurate measurement of the mass flow from the metre – which will be vital in the performance analysis of the overall resorption system.

An overall heat balance was also conducted on the fill region based on the thermal masses of the system and the NaBr salt reacting with the ammonia, which was compared to the integrated heat balance for the reactor. The results gave a satisfactory result, with values that were with 1% of one another.

Manganese chloride reactor (HTS)

A similar test of the ammonia mass flow metre was conducted with the manganese chloride reactor, however, with the nature of resorption

Fig. 22. Image of the proof-of-concept resorption experimental rig in front of the ThermExS thermal test facilities at Warwick, prior to manufacture of the ENG-salt sections and subsequent welding of the reactors.
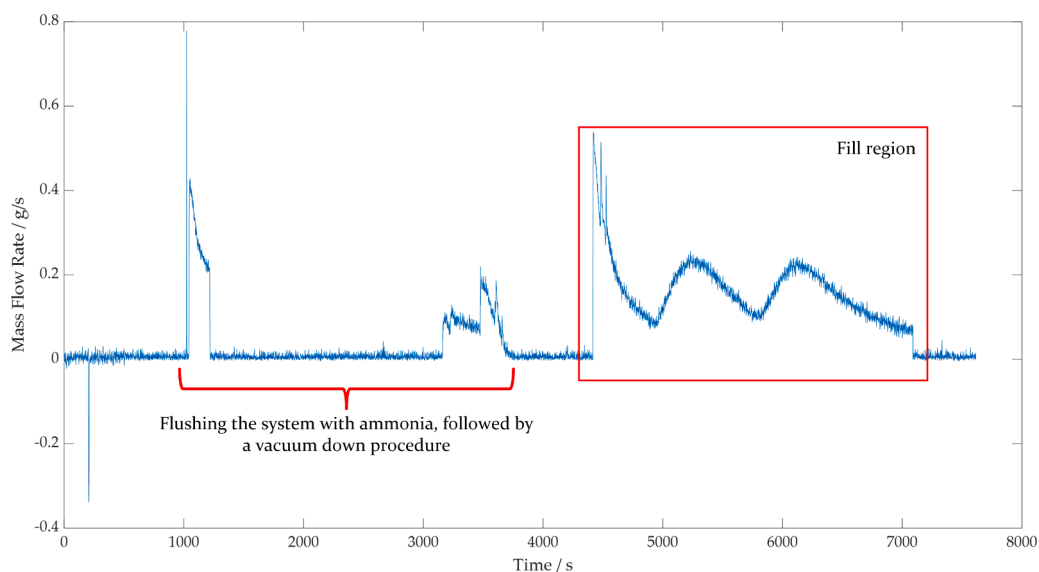
Fig. 23. Plot showing the ammonia mass flow rate versus time for the flushing, vacuum down and filling procedure for the sodium bromide LTS reactor. When integrating the 'fill region' signal, the filling mass matches that of the difference in mass of the ammonia bottle used to fill the rig.
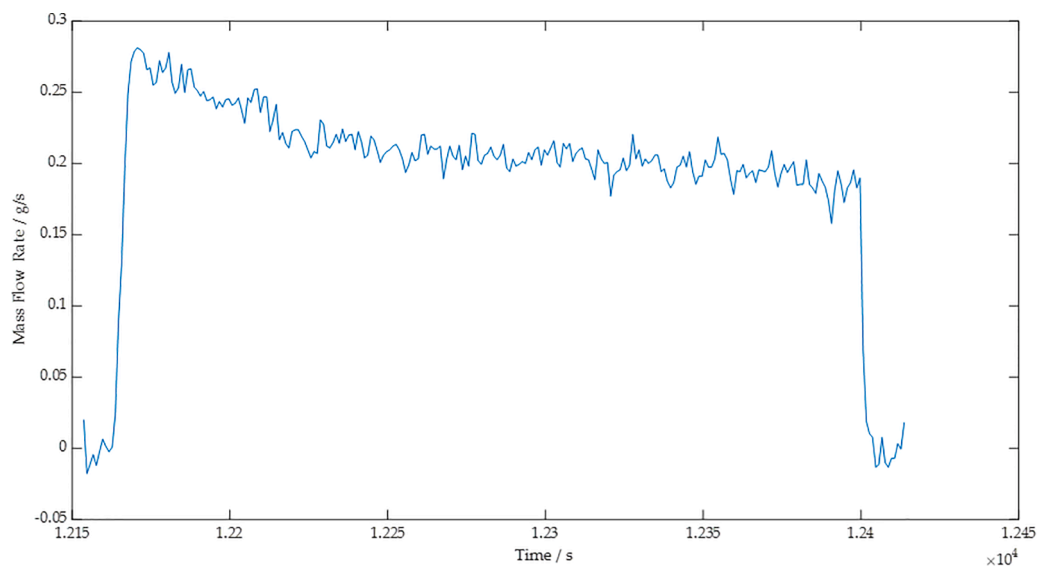

Fig. 24. Plot showing the ammonia mass flow rate versus time for the flushing of the manganese chloride HTS reactor. When integrating the 'fill region' signal, the filling mass matches that of the difference in mass of the ammonia bottle used to flush the reactor.

having one reactor ammoniated and the opposite reactor fully de-ammoniated, the $MnCl_2$ reactor was flushed with ammonia, rather than filled, and then evacuated. During the flush, again the ammonia bottle mass was monitored with the mass difference compared against the integrated signal from the Coriolis mass flow metre, Fig. 24. The mass difference of the bottle was 50 g_{NH3}, which was matched by the integrated signal of 50.1 g_{NH3}.

Conclusions

A proof-of-concept resorption system has been designed, manufactured and commissioned, with the first tests of the system being to assess the ammonia mass flow metre during filling and flushing of the LTS (sodium bromide) and HTS (manganese chloride) reactors. The validity of the ammonia mass flow data acquisition was checked against the physical measurement of the ammonia bottle mass when filling and

flushing the LTS and HTS reactors respectively.

The reactor (sorption heat exchanger) design has been informed by experimental analysis of Large Temperature Jump (LTJ) tests of the ENG-salt composite in a representative 'unit cell' reactor – subjecting the composite samples to conditions expected to be experienced in the full-scale resorption tests. The HTS ($MnCl_2$) results have been reproduced from (Hinmers et al., 2022) for completeness, with the LTS (NaBr) results reported in this work. The sodium bromide results show a marginal hysteresis band not seen in prior studies and the final reported adsorption and desorption enthalpy and entropy values for the 'equilibrium' line are as follows: $\Delta H_{ADS} = 30,102.5$ J/mol; $\Delta S_{ADS} = 207.7$ J/(mol·K); $\Delta H_{DES} = 30,216.4$ J/mol; and $\Delta S_{DES} = 206.8$ J/(mol·K). Modelling constants are also reported.

Future work

Future work on the resorption heat pump system will be to operate at a series of temperature conditions for the three defined working temperature levels described in this work. The results will enable the performance (COP and power) of the system to be analysed under steady state conditions. Analysis of the COP and power will inform the overall system performance against initial calculations and enable refinement of system cycle times to reach an optimum operating condition.

Analysing the results will also provide insight into the impact of the thermal masses in the reactor design on the COP, which may offer the biggest limitation on the successful performance of the resorption heat pump system. Additionally, with the welded reactor design, although the approach ensures that endplates and manifold thermal masses can be comparatively small compared to that of a flanged reactor design, the state of the composite salt adsorbent cannot easily be inspected. Therefore, insight into the state of the composite salt as future resorption tests progress may be missed and remarks on composite salt cycle stability may not be able to be drawn conclusively.

Declaration of Competing Interest

The authors declare that they have no known competing financial interests or personal relationships that could have appeared to influence the work reported in this paper.

Data availability

Data will be made available on request.

Appendix A

Halide Salt ΔH and ΔS Values

Table 5

Data collated from (G.L. An et al., 2019; Neveu and Castaing, 1993; Lepinasse and Spinner, January 1994; Li et al., 2014) to generate Fig. 2.

Salt	M.W./(g/mol)	Reaction Heat (ΔH)/(J/mol)	Reaction Entropy (ΔS)/(J/(mol·K))
NH_3 L/V	17.03	22,863	191.6
KI (4–0)	166.00	32,015	219.8
LiBr (5–4)	86.85	33,689	225.9
NH_4Cl (3–0)	53.49	29,433	207.9
$PbCl_2$ (8–3.25)	278.11	34,317	223.6
CaI_2 (8–6)	293.89	35,991	229.3
NaBr (5.25–0)	102.89	35,363	225.2
$BaCl_2$ (8–0)	208.23	38,250	232.4
$PbBr_2$ (5.5–3)	367.01	37,665	229.4
LiCl (4–3)	42.39	36,828	224.6
BaI_2 (6–4)	391.14	46,454	231.6
BaI_2 (4–2)	391.14	47,291	230.3
$MnCl_2$ (6–2)	125.84	47,416	228.1
$CaBr_2$ (6–2)	199.89	48,965	230.4
$FeCl_2$ (6–2)	126.75	51,266	228.0

Appendix B

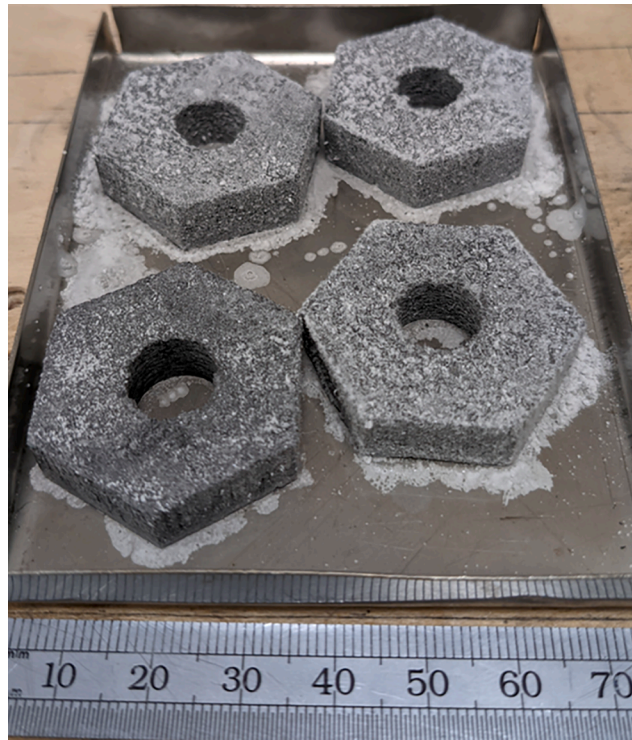Shell-side Reactor Reference Images

Fig. 25. Example of the hexagonal composite salt samples produced using the method described in Section 2.2.
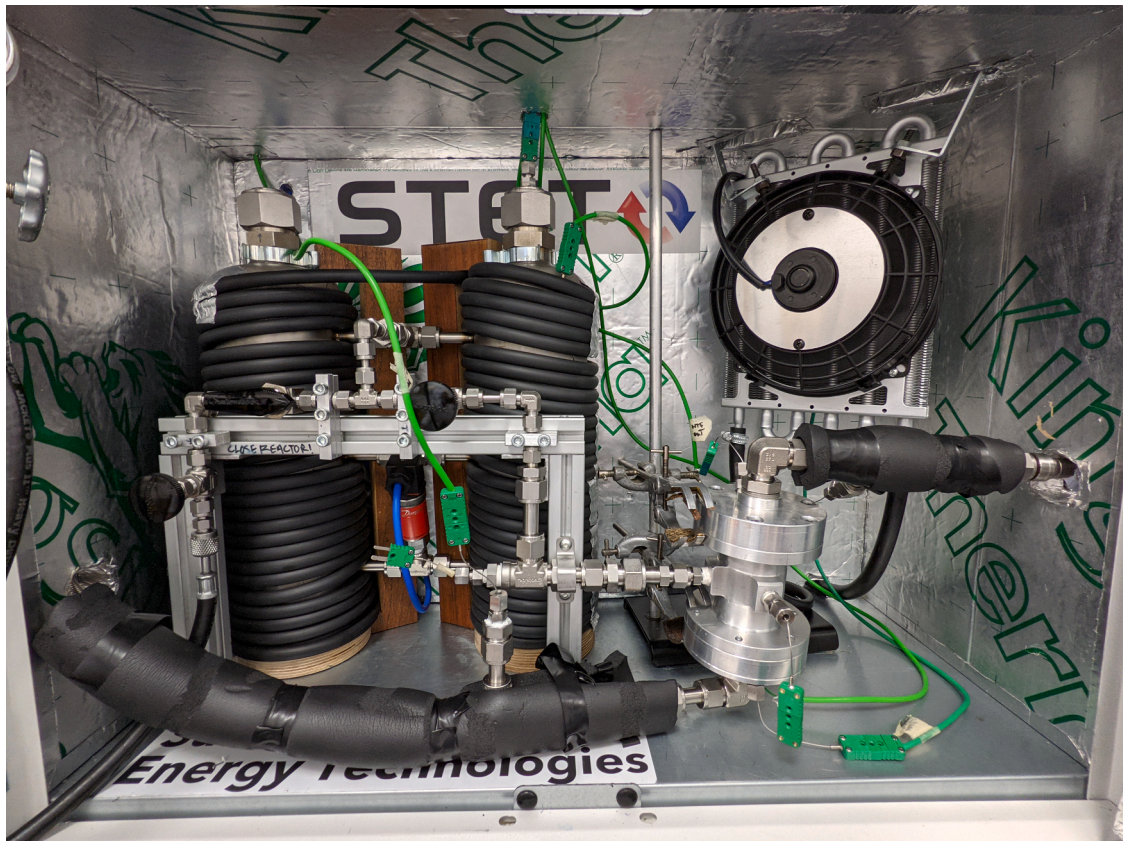

Fig. 26. The Large Temperature Jump (LTJ) shell-side experimental setup.

Appendix C

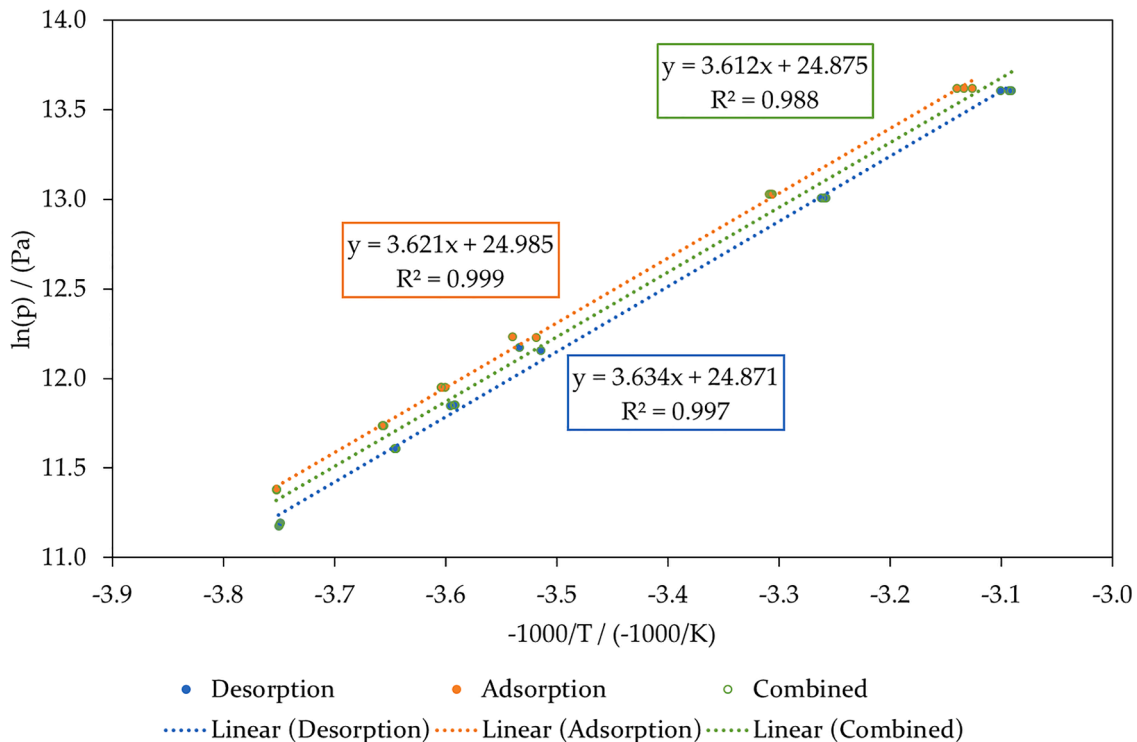Sodium Bromide Heat of Reaction

Fig. 27. Scatter graph for the adsorption (orange and round markers) and desorption (blue and square markers) across the sodium bromide tube side sample set tested, plotted with the combined data set and a single heat of reaction line (green). A linear regression line (dotted line) is plotted through the data set; the fits of 0.999, 0.997 and 0.988 respectively for adsorption (left), desorption (right) and combined (centre) indicate a strong positive correlation. The resulting line of best fit equation is also displayed for each data set. Refer to Fig. 10 for context.

References

Hinmers, S., Atkinson, G.H., Critoph, R.E., van der Pal, M., 2022a. Modelling and Analysis of Ammonia Sorption Reactions in Halide Salts. Int. J. Refrig. https://doi.org/10.1016/j.ijrefrig.2022.01.032.

Government, U.K., Trevelyan, A.-M., 2021. Say Hy to the Home of the Future. Department for Business, Energy & Industrial Strategy, London, UK.

UK Government, 2020. The Ten Point Plan for a Green Industrial Revolution. *Building Back better, Supporting Green jobs, and Accelerating Our Path to Net zero*, Department for Business, Energy & Industrial Strategy, Ed., ed. HM Government, London, UK.

Alefeld, G., 1975a. "Energiespeicherung durch heterogen-verdampfung. (II). Ein verfahren zur fernwaermespeicherung und spitzenstromerzeugung. (Energy storage by heterogenous evaporation. (II). A method of district heating storage with peak electricity generation),". Energie 27 (7–8), 180–183 volno.

Alefeld, G., 1975b. Energiespeicherung durch heterogen-verdampfung. I. Physikalish-technische grundlagen (Energy storage by heterogeneous evaporation. I. Technical and physical principles). Wärme 81 (5), 89–93 volno.

Metcalf, S., Rivero-Pacho, Á., Critoph, R., 2021a. Design and Large Temperature Jump Testing of a Modular Finned-Tube Carbon–Ammonia Adsorption Generator for Gas-Fired Heat Pumps. Energies 14 (11). https://doi.org/10.3390/en14113332.

Hinmers, S., Atkinson, G.H., Critoph, R.E., Van der Pal, M., 2022b. "Ammonia-Salt Reactions for Heat Pumping and Thermal Transforming Applications," Presented At the Heat Powered Cycles (HPC). Conference Paper, Bilbao, Spain, p. 313, 12th April.

Hinmers, S., Critoph, R.E., 2019. Modelling the ammoniation of barium chloride for chemical heat transformations. Energies 12 (23). https://doi.org/10.3390/en12234404.

Atkinson, G.H., Hinmers, S., Critoph, R.E., van der Pal, M., 2021. Ammonium Chloride (NH4Cl)—Ammonia (NH3): sorption Characteristics for Heat Pump Applications. Energies 14 (18). https://doi.org/10.3390/en14186002.

Hinmers, S., Atkinson, G.H., Critoph, R.E., van der Pal, M., 2022c. Resorption Thermal Transformer Generator Design. Energies 15 (6). https://doi.org/10.3390/en15062058.

van der Pal, M., Critoph, R.E., 2017. Performance of CaCl2-reactor for application in ammonia-salt based thermal transformers. Appl. Therm. Eng. 126, 518–524. https://doi.org/10.1016/j.applthermaleng.2017.07.086.

F. Ziegler, "Bond Energy," in *Energy Storage Systems*, vol. 2, Y. Gogus Ed. eBook: UNESCO - EOLSS, 2009, ch. 6.

Wang, R., Wang, L., Jingyi, W., 2014. Adsorption Refrigeration Technology Theory and Application. John Wiley & Sons, Singapore.

Bao, H., Ma, Z., Roskilly, A.P., 2018. Kinetic Models of Salt-Ammonia Chemisorption: an Overview and Comparison. *Chemisorption: Properties, Reactions and Uses*, M. Norup Ed. Nova Science Publishers, United States.

Goetz, V., Elie, F., Spinner, B., 1993. The structure and performance of single effect solid-gas chemical heat pumps. Heat Recovery Systems & CHP 13 (1), 79–96.

Yang, Z., Qu, M., Gluesenkamp, K.R., 2020. Ammonia-based chemisorption heat pumps for cold-climate heating applications: a comprehensive review. Appl. Therm. Eng. 179 https://doi.org/10.1016/j.applthermaleng.2020.115674.

Critoph, R.E., 1989. Activated carbon adsorption cycles for refrigeration and heat pumping. Carbon 27 (1), 63–70. https://doi.org/10.1016/0008-6223(89)90157-7.

Faraday, M., 1823. On the condensation of several gases into liquids. Philosophical Transactions of the Royal Society of London 113, 189–198 [Online]. Available. www.jstor.org/stable/107648.

Critoph, R.E., 2012. Solid sorption cycles: a short history. Int. J. Refrig. 35 (3), 490–493. https://doi.org/10.1016/j.ijrefrig.2012.02.007.

Goetz, V., Spinner, B., Lepinasse, E., 1997. A solid-gas thermochemical cooling system using BaCl2 and NiCl2,". Energy 22 (1), 49–58.

Lepinasse, E., Marion, M., Goetz, V., 2001. Cooling storage with a resorption process. Application to a box temperature control. Appl. Therm. Eng. 21 (12), 1251–1263. https://doi.org/10.1016/S1359-4311(00)00113-7.

Vasiliev, L.L., Mishkinis, D.A., Antukh, A.A., Kulakov, A.G., Vasiliev, L.L., 2004. Resorption heat pump. Appl. Therm. Eng. 24 (13), 1893–1903. https://doi.org/10.1016/j.applthermaleng.2003.12.018.

Worsøe-Schmidt, P., 1983. Solar refrigeration for developing countries using a solid-absorption cycle. Int. J. Ambient Energy 4 (3), 115–124. https://doi.org/10.1080/01430750.1983.9675877.

Gordeeva, L.G., Aristov, Y.I., 2012. Composites 'salt inside porour matrix' for adsorption heat transformations: a current state-of-the-art and new trends. Int. J. Low Carbon Technol. 7, 288–302. https://doi.org/10.1093/ijlct/cts050.

van der Pal, M., de Boer, R., Veldhuis, J.B.J., Smeding, S.F., 2009. Thermally driven ammonia-salt type II heat pump: development and test of a prototype. In: presented at the Heat Powered Cycles Conference. Berlin, Germany.

Oliveira, R.G., Wang, R.Z., Kiplagat, J.K., Wang, C.Y., 2009. Novel composite sorbent for resorption systems and for chemisorption air conditioners driven by low generation temperature. Renew Energy 34 (12), 2757–2764. https://doi.org/10.1016/j.renene.2009.05.016.

Li, T.X., Wang, R.Z., Kiplagat, J.K., Chen, H., 2010. Experimental study and comparison of thermochemical resorption refrigeration cycle and adsorption refrigeration cycle. Chem. Eng. Sci. 65 (14), 4222–4230. https://doi.org/10.1016/j.ces.2010.04.022.

Li, T.X., Wang, R.Z., Oliveira, R.G., Kiplagat, J.K., Wang, L.W., 2009. A combined double-way chemisorption refrigeration cycle based on adsorption and resorption processes. Int. J. Refrig. 32 (1), 47–57. https://doi.org/10.1016/j.ijrefrig.2008.07.007.

Li, T.X., Wang, R.Z., Kiplagat, J.K., Chen, H., Wang, L.W., 2011. A new target-oriented methodology of decreasing the regeneration temperature of solid–gas thermochemical sorption refrigeration system driven by low-grade thermal energy. Int. J. Heat Mass Transf. 54 (21–22), 4719–4729. https://doi.org/10.1016/j.ijheatmasstransfer.2011.06.005.

Li, T., Wang, R., Kiplagat, J.K., 2013. A target-oriented solid-gas thermochemical sorption heat transformer for integrated energy storage and energy upgrade. AlChE J. 59 (4), 1334–1347. https://doi.org/10.1002/aic.13899.

Xu, J., Oliveira, R.G., Wang, R.Z., 2011. Resorption system with simultaneous heat and cold production. Int. J. Refrig. 34 (5), 1262–1267. https://doi.org/10.1016/j.ijrefrig.2011.03.012.

Groll, M., 1993. Reaction beds for dry sorption machines. Heat Recovery Syst. CHP 13 (4), 341–346. https://doi.org/10.1016/0890-4332(93)90059-5, 1st July.

An, G.L., Wang, L.W., Gao, J., 2019a. Two-stage cascading desorption cycle for sorption thermal energy storage. Energy 174, 1091–1099. https://doi.org/10.1016/j.energy.2019.03.069.

Neveu, P., Castaing, J., 1993. Solid-gas chemical heat pumps: field of application and performance of the internal heat of reaction recovery process. Heat Recovery Systems & CHP 13 (3), 233–251.

Lepinasse, E., Spinner, B., 1994. Production de froid par couplage de réacteurs solide-gaz I: analyse des performances de tels systèmes. (Cold production through coupling of solid-gas reactors I: performance analysis). Int. J. Refrig. 17 (5), 309–322. https://doi.org/10.1016/0140-7007(94)90061-2, 1st January.

Li, T.X., Wang, R.Z., Li, H., 2014. Progress in the development of solid–gas sorption refrigeration thermodynamic cycle driven by low-grade thermal energy. Prog. Energy Combust. Sci. 40, 1–58. https://doi.org/10.1016/j.pecs.2013.09.002.

Hirata, Y., Fujioka, K., 2003. "Thermophysical properties and heat transfer characteristics of CaCl$_2$ heat pump reactor associated with structural change of reactive salts," presented at the Heat Pipes. In: Heat Pumps & Refrigerators Conference. Minsk, Belarus.

Aristov, Y.I., Dawoud, B., Glaznev, I.S., Elyas, A., 2008. A new methodology of studying the dynamics of water sorption/desorption under real operating conditions of adsorption heat pumps: experiment. Int. J. Heat Mass Transf. 51 (19–20), 4966–4972. https://doi.org/10.1016/j.ijheatmasstransfer.2007.10.042.

Mazet, N., Amouroux, M., Spinner, B., 1991. Analysis and experimental study of the transformation of a non-isothermal solid/gas reacting medium. Chem. Eng. Commun. 99 (1), 155–174. https://doi.org/10.1080/00986449108911585.

SGL Carbon. *SIGRATHERM® Graphite Lightweight Board*. [Online]. Available: https://www.sglcarbon.com/en/markets-solutions/material/sigratherm-graphite-lightweight-board/.

M. Furrer, "Thermoanalytical Study of Selected Complexes of Inorganic Chlorides With Ammonia and Ammonia Derivatives," Switzerland, 1980. Accessed: 22nd March 2020. [Online]. Available: http://inis.iaea.org/search/search.aspx?orig_q=RN:13652849.

Goetz, V., Marty, A., 1992. A model for reversible solid-gas reactions submitted to temperature and pressure contraints: simulations of the rate of reaction in solid-gas reactor used as chemical heat pump. Chem. Eng. Sci. 47 (17/18), 4445–4454.

An, G., Wang, L., Gao, J., Wang, R., 2019b. Mechanism of hysteresis for composite multi-halide and its superior performance for low grade energy recovery. Sci. Rep. 9 (1), 1563. https://doi.org/10.1038/s41598-018-38237-4. Feb 7.

Bao, H.S., Wang, R.Z., 2010. A Review of Reactant Salts for Resorption Refrigeration Systems. International Journal of Air-Conditioning and Refrigeration 18 (03), 165–180. https://doi.org/10.1142/s2010132510000150.

CALGAVIN, 2022. hiTRAN® Thermal Systems. https://www.calgavin.com/products-and-software/hitran-thermal-systems. accessed 15th October.

Raldow, W.M., Wentworth, W.E., 1979. Chemical heat pumps—A basic thermodynamic analysis. Sol. Energy 23 (1), 75–79. https://doi.org/10.1016/0038-092X(79)90046-X.

Metcalf, S.J., Rivero-Pacho, A.M., Critoph, R.E., 2021b. Design and Testing of a Carbon-Ammonia Gas-Fired Heat Pump. In: presented at the International Sorption Heat Pump Conference (ISHPC). Berlin, Germany (Virtual), p. 121.

Sustainable Thermal Energy Technologies (STET). "ThermExS Laboratory." The University of Warwick. https://warwick.ac.uk/fac/sci/eng/research/grouplist/sustainableenergy/facilities/thermxs/ (accessed 17th November 2019).